Self-consistent-field theories for complex fluids



1998 J. Phys.: Condens. Matter 10 8105

(http://iopscience.iop.org/0953-8984/10/37/002)

J. Phys.: Condens. Matter **10** (1998) 8105–8138. Printed in the UK PII: S0953-8984(98)88641-4

**REVIEW ARTICLE**

# Self-consistent-field theories for complex fluids

F Schmid

Institut für Physik, Universität Mainz, D-55099 Mainz, Germany

Received 11 May 1998

**Abstract.** Recent developments in off-lattice self-consistent-field theories for inhomogeneous complex fluids are reviewed. Particular emphasis is given to the treatment of intermolecular interactions and compressibility, to the role of fluctuations, and to the discussion of the coarse-graining length which is inherent to the theory. Valuable insight can be gained from the comparison of self-consistent-field calculations with Monte Carlo simulations. Finally, some applications of the theory to orientational properties of polymers and copolymers at interfaces, and to the phase behaviour of amphiphiles at surfaces, are presented.

## 1. Introduction

Surfaces and interfaces in supramolecular fluids are a topic of interest in various contexts of materials science and soft condensed matter physics.

On the one hand, the surface structure of materials determines many surface properties (adhesive and wetting properties, optical properties etc) and thus plays an important role for many applications, such as in lubricants, coatings, thin films and membranes [1, 2]. If the topography and chemistry of surfaces can be controlled, this can be exploited to design Taylor surfaces for specific purposes [3], e.g., surfaces which anchor liquid crystals in a well-defined way for liquid-crystal cells [4], intelligent surfaces [5] etc.

On the other hand, interfacial properties often influence the bulk behaviour of materials in a substantial way, since many commonly used materials are inhomogeneous on a microscopic scale. An important class of substances for which that is the case are melts of polymers which contain monomers of different type, e.g., polymer blends or copolymer melts. This is because different organic molecules are often slightly incompatible [6]. In homopolymer alloys (e.g., composite matrix materials such as rubber-toughened plastics), the small relative repulsion of the monomers is amplified by the large number of monomers in the macromolecules, and completely dominates the entropy of mixing, which is proportional to the number of molecules. As a result, polymers of different type are usually immiscible at temperatures of practical interest. They consist microscopically of numerous finely dispersed droplets of one component in the other, and the interfaces between these essentially unmixed phases largely govern the material properties [7–9].

One way to prevent the components from demixing is to chemically bind them to each other, thus forming block copolymers. Even though macroscopic phase separation is then inhibited, the chains still have a tendency to rearrange themselves so as to allow like monomers to pack next to each other. Depending on the temperature, block size etc, this may lead to 'microphase separation', i.e., the formation of ordered mesoscopic structures—of lamellae, ordered micelle arrays, bicontinuous structures [10]—which can be viewed as ordered arrays of interfaces in a sense. The properties of those materials strongly depend

0953-8984/98/378105+34$19.50  

on the topology and can be quite unusual [11, 12]. Copolymers are also used as effective compatibilizers in homopolymer blends. Added in small amounts, they reduce the interfacial tension between the homopolymer phases [13], and dynamically prevent the coalescence of droplets [14, 15]. Increasing the copolymer concentration results again in the formation of mesoscopically structured microphase-separated phases [16, 17].

Other prominent examples for inhomogeneous complex fluids are self-aggregating amphiphilic systems, e.g., mixtures of oil, water and soap, or lipid–water systems. At high enough amphiphile concentration, they build ordered structures which are very similar to the above-mentioned copolymer mesophases [18, 19]. The study of lipids in water is particularly interesting because of the close connection to biological physics. Indeed, bilayers of lipid molecules are a major ingredient of biological membranes and thus omnipresent in any living organism.

Complex fluids are typically made of chemically complicated, large molecules. They are usually characterized by a variety of competing length scales—in the case of polymer melts the size of the monomers versus the extension of whole molecules, in the case of amphiphilic systems also the correlation within and between the self-aggregated structures—and by the presence of additional, conformation and/or orientational, degrees of freedom. A full treatment in atomistic detail is in most cases out of reach of today's supercomputers. On the other hand, the apparent complexity of the systems actually contributes to a simplification of the physics on a coarse-grained level. Due to the large number of possible interactions between molecules, microscopic details average out to a large extent. A few characteristic attributes of the molecules are often responsible for the main features of a substance. For example, the properties of polymeric materials are determined mostly by the chain character and the flexibility of the polymers; amphiphilic systems are characterized by the affinity of their amphiphiles to both polar and nonpolar environments, and by their orientation at interfaces. This motivates the study of idealized simplified models, which account only for the main properties of the molecules and absorb the microscopic details in a few, effective parameters [20–22, 41, 42]. A second important point is that dense macromolecular systems are often unusually well described by mean-field approximations. Since large molecules interact with many others, the effective interaction range in the limit of high molecular weight is very large, and according to a simple Ginzburg-type argument, the critical region in which concentration fluctuations become important is very small as a result [23].

Mean-field theories are thus widely used to describe inhomogeneous macromolecular systems. Many simple and largely successful theories are based on Ginzburg–Landau-type functionals of the concentration or other extensive quantities (fields), which characterize a system with respect to the problem of interest [24]. The interactions between molecules are effectively incorporated into square-gradient terms and sometimes contributions of higher-order derivatives of the fields [19] The parameters of the model are either derived from a microscopic theory (as in the de Gennes–Flory–Huggins theory of inhomogeneous polymer mixtures [21]), or from comparison with experiment. Such a treatment is adequate as long as the interactions are short ranged, and the inhomogeneities are only weak and characterized by length scales of the order of the molecular size. It becomes questionable in systems which are inhomogeneous on smaller length scales—which is true for most examples cited above. A substantial amount of effort has therefore been put into developing more refined mean-field theories, which explicitly account for the chain conformational structure (lattice theories such as the Flory–Huggins theory [25, 20, 26, 27], density functional theories [28–31], self-consistent-field theories [32–36]), or even for the local structure in polymer melts (e.g., the lattice cluster theory given by Freed and co-workers [37], or the P-RISM theory given by Schweizer and Curro [38]). The more microscopic factors a theory incorporates, the more

detailed is the information that it can provide on local structure properties. Unfortunately, the treatment also gets more and more involved. Theories with a higher level of coarse graining have the advantage of being somewhat more transparent and easier to handle. Moreover, the origins of given physical phenomena can sometimes be tracked down more easily, if they can be discussed in terms of a highly idealized model. The optimal choice of a theory of course depends on the specific questions that one wishes to address.

In this paper, we shall discuss one of the most powerful mean-field tools in the study of macromolecular systems, the self-consistent-field approach. Even though, strictly speaking, every mean-field approximation involves self-consistent fields, the name self-consistent-field (SCF) theory is in the polymer community by tradition reserved for a certain type of approach, which dates back some time to the work of Edwards [39] and Helfand and Tagami [32]. In a nutshell, it can be characterized as follows. Polymers are described as random walks in a position-dependent chemical potential, which depends in turn in some self-consistent way on the distribution of monomers. The basic idea is thus extremely simple, which explains the enormous appeal that it has had for polymer scientists ever since it was first formulated. A particularly popular version of the theory has been developed by Scheutjens and Fleer for lattice models [36] and applied to various problems related to polymers at interfaces or surfaces [40]. Lattice models allow for an efficient study of systems with a planar geometry, as long as one is not crucially interested in chain stiffness and local orientation effects. The treatment of situations which involve strongly curved interfaces and local or global orientational order is more difficult. One way out of this dilemma is to employ more sophisticated lattice models. For example, the bond-fluctuation model of Carmesin and Kremer [43], a popular lattice model in Monte Carlo simulations [41, 44], has recently been used for self-consistent-field studies of lipid bilayers and polymer alloy systems [46]. On the other hand, the above-mentioned difficulties are automatically eliminated if one works in continuous space. We shall restrict our discussion mostly to such off-lattice models in the following. The basic concepts and recent methodical advances will be reviewed in the next section. In section 3, some applications will be presented which illustrate the use of the model for the study of polymer interfaces and amphiphilic systems. We summarize and conclude in section 4.

## 2. Theory

### *2.1. Basic concepts*

We consider a mixture of $n_j$ molecules of type $j = \mathrm{a}, \mathrm{b}, \mathrm{c}, \ldots$ in a volume $V$, which are built from $N_j$ monomers of species $\alpha = \mathrm{A}, \mathrm{B}, \mathrm{C}, \ldots$. Here Roman indices distinguish between molecule types, and Greek indices denote monomer species. For simplicity, we shall also assume that the monomers in a molecule build a linear sequence—the generalization to different architectures is straightforward [45]. The molecules can then be represented by continuous-space curves $\boldsymbol{R}(s)$, with $s$ varying between 0 and $N_j$. Polymer types $j$ differ from each other in their chain lengths $N_j$, and in the distributions of monomers $\alpha$ on the chains. The latter are conveniently described by functions $\gamma_{\alpha,j}(s)$, which are 1 for portions of the polymer occupied by the $\alpha$-monomers, and 0 otherwise. Hence one has

$$\sum_{\alpha} \gamma_{\alpha,j}(s) = 1$$

for all $j$ and $s$. In A homopolymers, for example, $\gamma_{\alpha}(s) = \delta_{\mathrm{A},\alpha}$ for all $s \in [0, N_j]$, and in the case of symmetric A:B diblock copolymers, $\gamma_{\alpha}(s) = \delta_{\mathrm{A},\alpha}$ for $s \in [0, N_j/2]$ and $\gamma_{\alpha}(s) = \delta_{\mathrm{B},\alpha}$ for $s \in [N_j/2, 1]$.

For a given configuration $\{\boldsymbol{R}_{i_j}(\cdot)\}$, one can then define a local monomer density operator

$$\widehat{\rho}_\alpha(\boldsymbol{r}) = \sum_j n_j \widehat{\rho}^j_\alpha(\boldsymbol{r}) \tag{1}$$

with

$$\widehat{\rho}^j_\alpha(\boldsymbol{r}) = \frac{1}{n_j}\sum_{i_j=1}^{n_j}\int_0^{N_j} \mathrm{d}s\ \delta(\boldsymbol{r}-\boldsymbol{R}_{i_j}(s))\gamma_{\alpha,j}(s).$$

The interaction between monomers can be described by a coarse-grained monomer free-energy functional $\mathcal{V}\{\widehat{\rho}_\alpha\}$. In addition to the Boltzmann factor associated with this interaction energy, chain conformations are distributed according to an intrinsic statistical weight $\mathcal{P}_j\{\boldsymbol{R}(\cdot)\}$, which accounts for the internal energy of the chain, and for the part of the configurational entropy which stems from length scales smaller than the coarse-graining length. In practice, polymers are most commonly modelled as Gaussian chains [47]:

$$\mathcal{P}_j\{\boldsymbol{R}(\cdot)\} = \mathcal{N}\exp\left[-\sum_\alpha \frac{3}{2b_\alpha^2}\int_0^{N_j}\mathrm{d}s\ \left|\frac{\mathrm{d}\boldsymbol{R}(s)}{\mathrm{d}s}\right|^2\gamma_{\alpha,j}(s)\right] \tag{2}$$

with the statistical segment length of $\alpha$-monomers $b_\alpha$, and the normalization factor $\mathcal{N}$ chosen such that

$$\int \mathcal{D}\{\boldsymbol{R}(\cdot)\}\ \mathcal{P}_j\{\boldsymbol{R}(\cdot)\} = V.$$

Here and in the following, all lengths are given in units of some microscopic length $V_0^{1/3}$ and are hence dimensionless. The conformational free energy of the chains is thus approximated by a Gaussian stretching energy with spring constant $3/2b_\alpha^2$. Shorter or stiffer polymers are sometimes represented as 'wormlike' chains of fixed contour length. Chain portions made up of $\alpha$-monomers are then characterized by the monomer length $a_\alpha$ and the dimensionless stiffness $\eta_\alpha$, and the probability distribution functionals $\mathcal{P}_j$ are given by [48]

$$\mathcal{P}_j\{\boldsymbol{R}(\cdot)\} = \mathcal{N}\prod_s \delta(\boldsymbol{U}^2-1)\exp\left[-\sum_\alpha\frac{\eta_\alpha}{2}\int_0^{N_j}\mathrm{d}s\ \left|\frac{\mathrm{d}\boldsymbol{U}(s)}{\mathrm{d}s}\right|^2\gamma_{\alpha,j}(s)\right] \tag{3}$$

where $\boldsymbol{U} = (\mathrm{d}\boldsymbol{R}/\mathrm{d}s)/a_\alpha$ is a dimensional tangent vector constrained to have magnitude unity by the delta function. This choice of a statistical weight has the advantage that monomer orientations are well defined, and orientation-dependent interactions between monomers can be introduced in a straightforward way. In the limit of small $\eta$, i.e., very flexible chains, the wormlike or semiflexible chain statistics reduces to Gaussian chain statistics [49]. Of course, it is also possible to consider chains with mixed Gaussian and wormlike parts.

Alternatively, many polymer models describe molecules in terms of discrete walks $\{\boldsymbol{R}_s\}$ instead of continuous curves $\{\boldsymbol{R}(s)\}$. The treatment is essentially the same, save that the integrals $\int_0^{N_j}\mathrm{d}s$ are replaced by sums $\sum_s$. In the case of freely jointed chains with fixed bond length $l$, for example, the statistical weight is

$$\mathcal{P}_j\{\boldsymbol{R}(\cdot)\} = \mathcal{N}\prod_{s=1}^{N_j-1}\delta\big(|\boldsymbol{R}_{s+1}-\boldsymbol{R}_s|-l\big). \tag{4}$$

The introduction of bending potentials acting on the angle between subsequent bonds, monomer-dependent bond lengths $l_{\alpha\beta}$ (for bonds connecting monomers $\alpha$ and $\beta$), or variable bond lengths with bond-length potentials, etc, is straightforward.

In all of the examples quoted so far, the chain statistics is determined by local relations between neighbour monomers along the chain, and is thus that of random walks. As we shall

see in section 2.2, solving such a model in the self-consistent-field approximation amounts to solving a diffusion equation self-consistently, which can usually be done at relatively moderate expense. This makes this kind of approach particularly attractive. However, the self-consistent-field method is not restricted to locally defined weight functions. Szleifer and co-workers [50, 51] have recently devised a procedure which allows one to perform self-consistent-field calculations for chains with arbitrary chain statistics, e.g., self-avoiding-walk statistics etc (see section 2.2).

In the following, we shall use the notation

$$\int \widehat{\mathcal{D}}_j\{\boldsymbol{R}(\cdot)\} = \int \mathcal{D}\{\boldsymbol{R}(\cdot)\}\ \mathcal{P}_j\{\boldsymbol{R}(\cdot)\}$$

for the weighted sum over all chain conformations, which is a path integral in the case of continuous curves, and a summation over discrete walks otherwise. The partition function of the system in the canonical ensemble is then given by

$$\mathcal{Z}_C = \prod_j \left\{ \frac{1}{n_j!} \prod_{i_j=1}^{n_j} \int \widehat{\mathcal{D}}_j\{\boldsymbol{R}_{i_j}(\cdot)\} \right\} \exp[-\beta \mathcal{V}\{\widehat{\rho}_\alpha\}] \tag{5}$$

where $\beta = 1/k_{\mathrm{B}}T$ is the Boltzmann factor, and the monomer interaction functional $\mathcal{V}\{\widehat{\rho}_\alpha\}$ has been introduced earlier. In order to proceed, it is useful [34] to insert functional integrals over delta functions

$$\mathbf{1} = \int \mathcal{D}\{\rho_\alpha\}\ \delta(\rho_\alpha - \widehat{\rho}_\alpha) = \int \mathcal{D}\{\rho_\alpha\} \int_{\mathrm{i}\infty} \mathcal{D}\{\omega_\alpha\}\ \exp\left( \int \mathrm{d}\boldsymbol{r}\ \omega_\alpha(\boldsymbol{r})(\rho_\alpha(\boldsymbol{r}) - \widehat{\rho}_\alpha(\boldsymbol{r})) \right) \tag{6}$$

which allow one to replace the density operators $\widehat{\rho}_\alpha(\boldsymbol{r})$ in $\mathcal{V}\{\widehat{\rho}_\alpha\}$ by density functions $\rho_\alpha(\boldsymbol{r})$. The subscript $\int_{\mathrm{i}\infty}$ indicates that the limits of integration of the auxiliary fields $\omega_\alpha(\boldsymbol{r})$ are $-\mathrm{i}\infty$ and $\mathrm{i}\infty$. Equation (5) can then be rewritten exactly as

$$\mathcal{Z}_C = \left\{ \prod_\alpha \int \mathcal{D}\{\rho_\alpha\} \int_{\mathrm{i}\infty} \mathcal{D}\{\omega_\alpha\} \right\} \exp[-\beta \mathcal{F}_C\{\rho_\alpha, \omega_\alpha\}] \tag{7}$$

with the canonical free-energy functional

$$\beta \mathcal{F}_C\{\rho_\alpha, \omega_\alpha\} = \beta \mathcal{V}\{\rho_\alpha\} - \sum_\alpha \int \mathrm{d}\boldsymbol{r}\ \omega_\alpha(\boldsymbol{r})\rho_\alpha(\boldsymbol{r}) - \sum_j n_j \ln(\mathcal{Q}_j\{\omega_\alpha\}/n_j). \tag{8}$$

The functional $\mathcal{Q}_j\{\omega_\alpha\}$ is the partition function of a single chain moving in the (imaginary) external fields $\omega_\alpha(\boldsymbol{r})$:

$$\mathcal{Q}_j\{\omega_\alpha\} = \int \widehat{\mathcal{D}}_j\{\boldsymbol{R}(\cdot)\}\ \exp\left[ -\sum_\alpha \int_0^{N_j} \mathrm{d}s\ \omega_\alpha(\boldsymbol{R}(s))\gamma_{\alpha,j}(s) \right]. \tag{9}$$

The main step of the self-consistent-field approach consists in performing a saddle-point integration of the integral (7) with respect to $\omega_\alpha(\boldsymbol{r})$: the path integral is replaced by the value of the integrand at the corresponding saddle function $\omega_\alpha(\boldsymbol{r})$ in the complex plane. Extremization of the exponent in (7) yields the equations

$$\rho_\alpha(\boldsymbol{r}) = -\sum_j n_j \frac{\delta \ln(\mathcal{Q}_j\{\omega_\alpha\})}{\delta \omega_\alpha(\boldsymbol{r})} = \langle \widehat{\rho}_\alpha(\boldsymbol{r}) \rangle_C. \tag{10}$$

The brackets $\langle \cdots \rangle_C$ denote statistical averages taken in a canonical ensemble of $n_j$ non-interacting chains of type $j$ subject to the external fields $\omega_\alpha(\boldsymbol{r})$. Note that the saddle functions $\omega_\alpha(\boldsymbol{r})$ which solve these equations are now real. The approximation thus amounts to replacing the exact constraint $\rho_\alpha(\boldsymbol{r}) = \widehat{\rho}_\alpha(\boldsymbol{r})$ in equation (6) by the more relaxed

requirement $\rho_\alpha(\boldsymbol{r}) = \langle\widehat{\rho}_\alpha(\boldsymbol{r})\rangle_C$. The functions $\omega_\alpha(\boldsymbol{r})$ act as Lagrange parameters which enforce this condition. The resulting partition function is

$$\mathcal{Z}_C = \left\{\prod_\alpha \int \mathcal{D}\{\rho_\alpha\}\right\} \exp[-\beta\mathcal{F}_C\{\rho_\alpha, \omega_\alpha\{\rho_\alpha\}\}] \tag{11}$$

where the fields $\omega_\alpha\{\rho_\alpha\}$ depend self-consistently on $\rho_\alpha$ according to equation (10).

When looking at mixtures, it is sometimes more convenient to work in the grand canonical ensemble [35, 52]. The starting point is then the grand canonical partition function

$$\mathcal{Z}_{GC} = \prod_j \sum_{n_j=0}^{\infty} \left\{\frac{\mathrm{e}^{\beta\mu_j n_j}}{n_j!} \prod_{i_j=1}^{n_j} \int \widehat{\mathcal{D}}_j\{\boldsymbol{R}_{i_j}(\cdot)\}\right\} \exp[-\beta\mathcal{V}\{\widehat{\rho}_\alpha\}] \tag{12}$$

where the $\mu_j$ are the chemical potentials associated with molecules of type $j$. One can now proceed in the same way as above, and obtain the analogue to (7) with the grand canonical free-energy functional:

$$\beta\mathcal{F}_{GC}\{\rho_\alpha, \omega_\alpha\} = \beta\mathcal{V}\{\rho_\alpha\} - \sum_\alpha \int \mathrm{d}\boldsymbol{r}\ \omega_\alpha(\boldsymbol{r})\rho_\alpha(\boldsymbol{r}) - \sum_j \mathrm{e}^{\beta\mu_j}\mathcal{Q}_j\{\omega_\alpha\}. \tag{13}$$

The extremization with respect to $\omega_\alpha(\boldsymbol{r})$ yields the condition

$$\rho_\alpha(\boldsymbol{r}) = -\sum_j \mathrm{e}^{\beta\mu_j}\frac{\delta\mathcal{Q}_j}{\delta\omega_\alpha(\boldsymbol{r})} = \left\langle\widehat{\rho}_\alpha(\boldsymbol{r})\right\rangle_{GC}. \tag{14}$$

Hence the grand canonical partition function in the self-consistent-field approximation reads

$$\mathcal{Z}_{GC} = \left\{\prod_\alpha \int \mathcal{D}\{\rho_\alpha\}\right\} \exp[-\beta\mathcal{F}_{GC}\{\rho_\alpha, \omega_\alpha\{\rho_\alpha\}\}] \tag{15}$$

with $\omega_\alpha\{\rho_\alpha\}$ defined via equation (14).

At this point, concentration fluctuations are still included in the partition function. Usually, self-consistent-field approximations take one more step and perform a second saddle-point integration of (11) or (15) with respect to $\rho_\alpha(\boldsymbol{r})$. The free energy is then approximated by

$$F = -k_\mathrm{B}T\ln\mathcal{Z} \approx F^{SCF} = \min_{\rho_\alpha(\boldsymbol{r})} \mathcal{F}\{\rho_\alpha, \omega_\alpha\{\rho_\alpha\}\} \tag{16}$$

with the minimization equations

$$\omega_\alpha(\boldsymbol{r}) = \frac{\delta\beta\mathcal{V}}{\delta\rho_\alpha(\boldsymbol{r})} \tag{17}$$

in both the canonical and the grand canonical ensemble. This is a very intuitive, typical mean-field result: the auxiliary fields $\omega_\alpha(\boldsymbol{r})$ which drive the monomer densities $\rho_\alpha(\boldsymbol{r})$ are identified with the local excess free energy needed to add one monomer $\alpha$ to the melt at the position $\boldsymbol{r}$, less the contribution of the translational entropy of polymers. Since the fields $\omega_\alpha$ are functions of $\rho_\alpha$ by means of equation (10) or (14), equation (17) effectively determines the mean-field concentration profiles $\rho_\alpha^{SCF}(\boldsymbol{r})$.

Hence two approximations enter the self-consistent-field theory: the first leading to equation (11) or equation (15), respectively, and the second leading to equation (16). We have taken care to separate these two steps for the following reasons. First, Shi, Noolandi and Desai [53] have recently suggested a way to systematically improve on the second step and take Gaussian or even higher-order concentration fluctuations into account (see section 2.4). This allows for a stability analysis of the mean-field solution [54], and for the construction of kinetic paths connecting different mean-field solutions [55]. Second, the two

steps differ qualitatively from each other. Technically, the saddle functional approximates integrals of $\omega_\alpha$ on the imaginary axis, and real integrals of $\rho_\alpha$. A stable saddle point is thus a *minimum* with respect to $\rho_\alpha$ and a *maximum* with respect to $\omega_\alpha$. The first step motivates the introduction of a coarse-grained density functional $\mathcal{F}\{\rho_\alpha, \omega_\alpha\{\rho_\alpha\}\}$, which is then minimized in step two as in usual mean-field approaches.

The introduction of orientation-dependent monomer interactions into the formalism is straightforward. The monomer density operator (1) is simply replaced by

$$\widehat{\rho}^j_\alpha(\boldsymbol{r}, \boldsymbol{u}) = \frac{1}{n_j} \sum_{i_j=1}^{n_j} \int_0^{N_j} \mathrm{d}s\ \delta(\boldsymbol{r} - \boldsymbol{R}_{i_j}(s))\delta(\boldsymbol{u} - \boldsymbol{U}_{i_j}(s))\gamma_{\alpha,j}(s) \tag{18}$$

where $\boldsymbol{U}$ is the orientation of monomer $i_j$. The fields $\omega_\alpha$ become orientation dependent and meet (cf. (17)) $\omega_\alpha(\boldsymbol{r}, \boldsymbol{u}) = \delta\beta\mathcal{V}/\delta\rho_\alpha(\boldsymbol{r}, \boldsymbol{u})$.

Finally in this section, we sketch Helfand's original formulation of the self-consistent-field theory [33], which is particularly suited for the study of polymer interfaces and surfaces. Consider an interface between two entirely segregated homopolymer phases $j = \mathrm{A}$ and B, which each occupy a partial volume $V_j = n_j N_j/\rho_j^*$. The two pure systems are characterized by their bulk densities $\rho_j^*$ and the associated fields $\omega_j^* = \mathrm{d}\nu_j^*/\mathrm{d}\rho_j^*$, where $\nu_j^*$ is the bulk density of the interaction energy $\mathcal{V}$. Let further the probability distribution $\mathcal{P}_j\{\boldsymbol{R}(\cdot)\}$ be normalized such that $\int \widehat{\mathcal{D}}_j\{\boldsymbol{R}(\cdot)\} = V_j$. The free-energy density of the pure systems is then given by

$$\beta f_j^* = \beta\nu_j^* + \rho_j^*/N_j \ln(\rho_j^*/N_j).$$

When looking at the interface between the two phases, it is now convenient to work with shifted monomer fields:

$$\tilde{\omega}_j(\boldsymbol{r}) = \omega_j(\boldsymbol{r}) - \omega_j^* \tag{19}$$

which vanish in the pure system $j$. They can be interpreted as the excess work needed to bring a monomer of type $j$ from the pure system into the interfacial region. The underlying shifted interaction potential ($\tilde{\omega}_j(\boldsymbol{r}) = \delta\tilde{\mathcal{V}}/\delta\rho_j(\boldsymbol{r})$) has the form

$$\beta\tilde{\mathcal{V}} = \beta\mathcal{V} - \sum_j \omega_j^* \int \mathrm{d}\boldsymbol{r}\ \rho_j(\boldsymbol{r}) - \text{constant} \tag{20}$$

where

$$\text{'constant'} = \sum_j V_j\{\beta\nu_j^* - \omega_j^*\rho_j^*\}$$

subtracts the bulk contribution of the pure phases. The shifted fields $\tilde{\omega}_j$ define a renormalized single-chain partition function:

$$\tilde{\mathcal{Q}}_j = \int \widehat{\mathcal{D}}_j\{\boldsymbol{R}(\cdot)\}\ \exp\left[-\int_0^{N_j} \mathrm{d}s\ \tilde{\omega}_j(\boldsymbol{R}(s))\right] = \mathcal{Q}_j \exp[-\omega_j^* N_j]. \tag{21}$$

Note that the actual value of $\tilde{\mathcal{Q}}_j$ is $\tilde{\mathcal{Q}}_j = n_j N_j/\rho_j^*$. Hence the equation for the density profiles can be written in the simple form

$$\rho_j(\boldsymbol{r}) = -\frac{\rho_j^*}{N_j} \frac{\delta\tilde{\mathcal{Q}}_j}{\delta\tilde{\omega}_j(\boldsymbol{r})} \tag{22}$$

and the excess free energy of the interface is

$$\beta F_{exc} = \beta\tilde{\mathcal{V}}\{\rho_j\} - \sum_j \int \mathrm{d}\boldsymbol{r}\ \tilde{\omega}_j(\boldsymbol{r})\rho_j(\boldsymbol{r}). \tag{23}$$

The formalism can also be applied if the polymers A and B are not fully segregated, i.e., the bulk phases contain both A and B. In that case, the interfacial free energy (23) has to be corrected for additional bulk contributions. Helfand *et al* have approximated the excess interaction potential $\tilde{\mathcal{V}}$ by the simple form [32, 33]

$$\beta\tilde{\mathcal{V}} = \int \mathrm{d}\boldsymbol{r} \left\{ \chi \frac{\rho_\mathrm{A}\rho_\mathrm{B}}{\sqrt{\rho_\mathrm{A}^*\rho_\mathrm{B}^*}} + \frac{1}{2\kappa k_\mathrm{B}T}\left(\frac{\rho_\mathrm{A}}{\rho_\mathrm{A}^*} + \frac{\rho_\mathrm{B}}{\rho_\mathrm{B}^*} - 1\right)^2 \right\} \tag{24}$$

where the Flory–Huggins parameter $\chi$ describes the incompatibility of monomers A and B, and $\kappa$ is the compressibility of the melt. In the limit of infinitely long polymers and zero compressibility, Helfand and Tagami were able to solve the theory analytically (SSL: strong-segregation limit [32]). For a symmetric mixture ($b_\mathrm{A} = b_\mathrm{B} = b$, $\rho_\mathrm{A}^* = \rho_\mathrm{B}^* = \rho$), they obtained the interfacial tension $\beta\sigma_{SSL} = \sqrt{\chi/6}\rho b$ and the interfacial width $w_{SSL} = b/\sqrt{6\chi}$.

### *2.2. Implementation*

Equations (10) or (14) and (17) define a complete cycle of self-consistent equations, which can be solved numerically by suitable iteration methods. The main task in each iteration step consists in evaluating the partition function $\mathcal{Q}_j\{\omega_\alpha\}$ of a single chain $j$ in the external fields $\omega_\alpha(\boldsymbol{r})$ (9) and the derivatives of $\mathcal{Q}_j\{\omega_\alpha\}$. If the polymers have random-walk statistics $\mathcal{P}_j\{\boldsymbol{R}(\cdot)\}$ as in (2), (3) or (4), it is useful to define the propagators

$$G_j(\boldsymbol{r}, t; \boldsymbol{r}', t') = \int \widehat{\mathcal{D}}_j\{\boldsymbol{R}(\cdot)\} \ \exp\left[ -\sum_\alpha \int_t^{t'} \mathrm{d}s \ \omega_\alpha(\boldsymbol{R}(s))\gamma_{\alpha,j}(s) \right] \times \delta(\boldsymbol{r} - \boldsymbol{R}(t))\delta(\boldsymbol{r}' - \boldsymbol{R}(t')) \tag{25}$$

or, in the case where monomer orientations are important,

$$G_j(\boldsymbol{r}, \boldsymbol{u}, t; \boldsymbol{r}', \boldsymbol{u}', t') = \int \widehat{\mathcal{D}}_j\{\boldsymbol{R}(\cdot)\} \ \exp\left[ -\sum_\alpha \int_t^{t'} \mathrm{d}s \ \omega_\alpha(\boldsymbol{R}(s))\gamma_{\alpha,j}(s) \right] \times \delta(\boldsymbol{r} - \boldsymbol{R}(t))\delta(\boldsymbol{r}' - \boldsymbol{R}(t'))\delta(\boldsymbol{u} - \boldsymbol{U}(t))\delta(\boldsymbol{u}' - \boldsymbol{U}(t')). \tag{26}$$

Since they carry no memory along the chain, these propagators satisfy modified diffusion equations with the initial condition

$$G_j(\boldsymbol{r}, t; \boldsymbol{r}', t) = \delta(\boldsymbol{r} - \boldsymbol{r}')$$

or

$$G_j(\boldsymbol{r}, \boldsymbol{u}, t; \boldsymbol{r}', \boldsymbol{u}', t') = \delta(\boldsymbol{r} - \boldsymbol{r}')\delta(\boldsymbol{u} - \boldsymbol{u}').$$

Specifically, the diffusion equation for Gaussian chains (2) reads [32]

$$\left[ \frac{\partial}{\partial t'} + \sum_\alpha \gamma_{\alpha,j}(t') \left[ -\frac{b_\alpha^2}{6}\nabla_{\boldsymbol{r}'}^2 + \omega_\alpha(\boldsymbol{r}') \right] \right] G_j(\boldsymbol{r}, t; \boldsymbol{r}', t') = 0. \tag{27}$$

For wormlike chains (3) [49],

$$\left[ \frac{\partial}{\partial t'} + \sum_\alpha \gamma_{\alpha,j}(t') \left[ a_\alpha \boldsymbol{u}'\nabla_{\boldsymbol{r}'} - \frac{1}{2\eta_\alpha}\nabla_{\boldsymbol{u}'}^2 + \omega_\alpha(\boldsymbol{r}') \right] \right] G_j(\boldsymbol{r}, \boldsymbol{u}, t; \boldsymbol{r}', \boldsymbol{u}', t') = 0 \tag{28}$$

and for freely jointed chains with bond length $l$ (4),

$$G_j(\boldsymbol{r}, t; \boldsymbol{r}', t' + 1) = \exp[-\omega_\alpha(\boldsymbol{r}')]\frac{1}{4\pi}\int \mathrm{d}\boldsymbol{u} \ G_j(\boldsymbol{r}, t; \boldsymbol{r}' - l\boldsymbol{u}, t') \tag{29}$$

where $|\boldsymbol{u}| = 1$ as before, and $\int \mathrm{d}\boldsymbol{u}$ denotes integration over the full solid angle. Once the propagators have been determined, one easily calculates the partition function

$$\mathcal{Q}_j = \int \mathrm{d}\boldsymbol{r}\ \mathrm{d}\boldsymbol{r}'\ G_j(\boldsymbol{r}, 0; \boldsymbol{r}', N_j)$$

and its derivatives

$$\frac{\delta \mathcal{Q}_j}{\delta \omega_\alpha(\boldsymbol{r}_0)} = \int \mathrm{d}\boldsymbol{r}\ \mathrm{d}\boldsymbol{r}' \int_0^{N_j} \mathrm{d}s\ \gamma_{\alpha,j}(s) G_j(\boldsymbol{r}, 0; \boldsymbol{r}_0, s) G_j(\boldsymbol{r}_0, s; \boldsymbol{r}', N_j) \tag{30a}$$

$$\frac{\delta^2 \mathcal{Q}_j}{\delta \omega_\alpha(\boldsymbol{r}_0)\, \delta \omega_\beta(\boldsymbol{r}_1)} = 2 \int \mathrm{d}\boldsymbol{r}\ \mathrm{d}\boldsymbol{r}' \int_0^{N_j} \mathrm{d}s\ \gamma_{\alpha,j}(s) \int_0^{s} \mathrm{d}s'\ \gamma_{\beta,j}(s') \times G_j(\boldsymbol{r}, 0; \boldsymbol{r}_0, s') G_j(\boldsymbol{r}_0, s'; \boldsymbol{r}_1, s) G_j(\boldsymbol{r}_1, s; \boldsymbol{r}', N_j) \tag{30b}$$

etc. In fact, only the first derivatives enter the self-consistent-field equations. It is thus often less time consuming to calculate directly the 'end-segment distributions'

$$q_j(\boldsymbol{r}, t) = \int \mathrm{d}\boldsymbol{r}'\ G_j(\boldsymbol{r}', 0; \boldsymbol{r}, t) \qquad \bar{q}_j(\boldsymbol{r}, t) = \int \mathrm{d}\boldsymbol{r}'\ G_j(\boldsymbol{r}, t; \boldsymbol{r}', N_j)$$

which solve the same diffusion equation as $G$ with boundary conditions $q_j(\boldsymbol{r}, 0) = 1$ and $\bar{q}_j(\boldsymbol{r}, N_j) = 1$. The end-segment distribution functions can be used to calculate density profiles, chain-end distributions etc. The full propagators $G_j(\boldsymbol{r}, t; \boldsymbol{r}', t')$ are needed when looking at the effect of fluctuations (see section 2.4), or at chain correlation functions such as distributions of end-to-end vectors.

Diffusion equations can usually be solved without too much computational effort. The computer time needed for one iteration step only scales linearly with the chain length $N$, and hence one can handle relatively long chains. Physically, treating the chains as random walks is well justified in dense melts of long polymers, since the excluded-volume interactions between monomers of the same chain are screened by the presence of other chains [21].

However, this is not true for dilute polymer chains, and on length scales smaller than the screening length [21]. The random-walk approximation thus becomes questionable when looking at polymers in good-solvent conditions, or at relatively short macromolecules. In that case, it is more appropriate to choose a weight distribution $\mathcal{P}_j$ which accounts also for long-range correlations within a chain. One then has to consider whole chains in the external field of the other chains (the single-chain mean field).

Szleifer and co-workers have recently suggested an enumeration procedure for the evaluation of chain partition functions [50, 51]. They approximate the path integral $\int \widehat{\mathcal{D}}_j\{\boldsymbol{R}(\cdot)\}$ by the sum over a representative sample of chain configurations $\boldsymbol{R}_{i_j}(\cdot)$, which are distributed according to the weight function $\mathcal{P}_j\{\boldsymbol{R}(\cdot)\}$. The sample can be generated by Monte Carlo simulations, taken from experiments etc. This approach is conceptually extremely simple and can be applied to arbitrary weight distributions $\mathcal{P}_j\{\boldsymbol{R}(\cdot)\}$. For example, dilute polymers in good solvent are well described by self-avoiding walks, and one can generate the sample from single-chain simulations [50]. Semidilute polymers have self-avoiding-walk statistics on short length scales below the screening length, and random-walk statistics on larger length scales. The best description on all length scales is obtained when the sample is generated in Monte Carlo simulations of a melt [46]. Unfortunately, the computational effort required to reliably solve the self-consistent equations grows rapidly with the chain length, since the sizes of the sample have to be made very large. In a dense melt of long polymers, random-walk models for chains usually give reasonably good results at much less expense.

Nevertheless, the method is very versatile and has much potential for further refinement. For example, reweighting schemes can be devised in analogy to the reweighting techniques

in Monte Carlo simulations [56], which are useful if the actual distribution of chain conformations differs substantially from the distribution $\mathcal{P}_j\{\boldsymbol{R}(\cdot)\}$. One then draws the sample of chain conformations according to a modified distribution $\mathcal{P}'_j\{\boldsymbol{R}(\cdot)\}$, and corrects for this in the sum over conformations:

$$\int \widehat{\mathcal{D}}_j\{\boldsymbol{R}(\cdot)\}\ \cdots \longrightarrow \sum_{\boldsymbol{R}_{i_j}} (\mathcal{P}_j\{\boldsymbol{R}_{i_j}(\cdot)\}/\mathcal{P}'_j\{\boldsymbol{R}_{i_j}(\cdot)\}) \cdots$$

Weinhold *et al* have introduced a coupling between $\mathcal{P}_j$ and the number of interchain contacts, and could qualitatively reproduce the shrinking of chains in an athermal melt with increasing monomer density [57]. Within a similar approach, Müller calculates the statistical mechanics of clusters of polymers embedded in a self-consistent field, in order to study the conformations of a single A chain in an unfavourable B environment [58]. His results compare well with Monte Carlo simulations.

With these remarks, we end the discussion of the Szleifer method. The reader is referred to [51] for a detailed review of the approach and its applications. We close this section with a few technical comments on the solution of the mean-field equations.

The careful choice of a suitable basis is crucial for the success of a self-consistent-field calculation. Matsen *et al* have implemented with great success a method for studying periodically ordered mesophases, where spatially dependent functions are expanded in orthonormal basis functions with the symmetry of the phase being taken into consideration [59–61]. If monomer interactions come into play, it is usually beneficial to expand functions of the orientation $\boldsymbol{u}$ in spherical harmonics [62].

The mean-field equations are solved iteratively, e.g., using the fields $\omega_\alpha(\boldsymbol{r})$ as iteration variables. The most popular iteration procedure is the Newton–Raphson method [63]. One usually obtains a solution of reasonably high accuracy within fewer than ten iteration steps. However, each step involves the determination of a full Hesse matrix of derivatives, i.e., the number of function evaluations grows quadratically with the number of degrees of freedom. Relaxation procedures take more iteration steps, but may nevertheless require fewer function evaluations in the end. The present author has had good experience with a variant of a method originally suggested by Ng [64, 65]. Another efficient procedure is the multidimensional secant method of Broyden [66, 67].

### *2.3. Monomer interactions and compressibility*

We now turn to the discussion of the functional $\mathcal{V}\{\rho_\alpha\}$, which defines together with $\mathcal{P}_j\{\boldsymbol{R}(\cdot)\}$ the actual model. It describes the free energy of a system of interacting monomers without translational entropy. Naively, one could be tempted to identify it with the sum of direct interactions $W_{\alpha\beta}(\boldsymbol{r})$ between monomers,

$$\frac{1}{2}\int \mathrm{d}\boldsymbol{r}\ \mathrm{d}\boldsymbol{r}'\ \sum_{\alpha\beta} W_{\alpha\beta}(\boldsymbol{r}-\boldsymbol{r}')\rho_\alpha(\boldsymbol{r})\rho_\beta(\boldsymbol{r}').$$

However, this approximation is poor for dense fluids, where indirect interactions and multiplet correlations are important. In most applications of the self-consistent-field theory, the quantities of interest are composition inhomogeneities, whereas the total density varies comparatively little throughout the system. Furthermore, the relative repulsion of monomers of different types is usually vanishingly small compared to the total free energy in the melt. It is thus propitious to separate $\mathcal{V}$ into an 'equation-of-state' contribution $\mathcal{V}_0$, which accounts for density fluctuations and compressibility effects, and an interaction part $\mathcal{V}_{\mathrm{inter}}$, which

incorporates the incompatibility of unlike monomers:

$$\mathcal{V}\{\rho_\alpha\} = \mathcal{V}_0\{\rho_\alpha\} + \mathcal{V}_{\text{inter}}\{\rho_\alpha\}. \tag{31}$$

We shall discuss the two parts in turn, and begin with $\mathcal{V}_0$. If the melt is nearly incompressible and the density fluctuations are small, one may use Helfand's quadratic approximation [32, 33] (see equation (24))

$$\mathcal{V}_0\{\rho_\alpha\} = \frac{1}{2\kappa}\int \mathrm{d}\boldsymbol{r}\,\left(1 - \sum_\alpha \rho_\alpha v_\alpha\right)^2 \tag{32}$$

where $v_\alpha$ is the specific volume of an $\alpha$-monomer.

More rigorously, total incompressibility is often postulated:

$$\sum_\alpha \rho_\alpha(\boldsymbol{r}) v_\alpha \equiv 1 \qquad \text{everywhere.} \tag{33}$$

This is most commonly achieved by introducing an additional Lagrange parameter field $\xi(\boldsymbol{r})$, which couples to the incompressibility constraint (33) [34, 35, 59]. The free-energy functional (8) or (13) is then replaced by

$$\begin{aligned}\beta\mathcal{F} = \beta\mathcal{V}_{\text{inter}}\{\rho_\alpha\} - \sum_\alpha \int \mathrm{d}\boldsymbol{r}\;\omega_\alpha(\boldsymbol{r})\rho_\alpha(\boldsymbol{r}) - \int \mathrm{d}\boldsymbol{r}\;\xi(\boldsymbol{r})\left[\sum_\alpha \rho_\alpha(\boldsymbol{r}) v_\alpha - 1\right] \\ - \begin{cases} \displaystyle\sum_j n_j \ln(\mathcal{Q}_j\{\omega_\alpha\}/n_j) & \text{(canonical ensemble)} \\ \displaystyle\sum_j \mathrm{e}^{\beta\mu_j}\mathcal{Q}_j\{\omega_\alpha\} & \text{(grand canonical ensemble)} \end{cases}\end{aligned} \tag{34}$$

and the minimization equation (17) turns into

$$\omega_\alpha(\boldsymbol{r}) = \frac{\delta\beta\mathcal{V}_{\text{inter}}}{\delta\rho_\alpha(\boldsymbol{r})} - \xi(\boldsymbol{r})v_\alpha. \tag{35}$$

The incompressibility constraint (33) determines the field $\xi(\boldsymbol{r})$ unambiguously, except for a constant $\xi_0$. It is often chosen such that $\int \mathrm{d}\boldsymbol{r}\;\xi(\boldsymbol{r}) = 0$. Note that the choice of $\xi_0$ determines the offset of the chemical potentials $\mu_j$ in the grand canonical ensemble.

Within this framework of an incompressible theory, total-density fluctuations are often reintroduced by means of a hypothetical noninteracting 'solvent' $s$, which fills the space between the molecules [34, 51, 68, 69]. The incompressibility condition (33) then reads

$$\sum_\alpha \rho_\alpha(\boldsymbol{r})v_\alpha + \rho_s(\boldsymbol{r})v_s \equiv 1$$

and the excess potential of the solvent is simply given by $\omega_s(\boldsymbol{r}) = \xi(\boldsymbol{r})v_s$. According to equation (10) or (14), the density of the solvent is thus given by

$$\rho_s(\boldsymbol{r}) = z\exp[-\xi(\boldsymbol{r})v_s]$$

with

$$z = n_s \Big/ \int \mathrm{d}\boldsymbol{r}\;\exp[-\xi(\boldsymbol{r})v_s]$$

in the canonical case and

$$z = \exp[\beta\mu_s]$$

in the grand canonical case. This defines $\xi(\boldsymbol{r})$ as a function of the monomer densities $\rho_\alpha(\boldsymbol{r})$. Choosing $\xi_0$ such that $\ln(zv_s) = 0$, one obtains the fields

$$\omega_\alpha(\boldsymbol{r}) = \frac{\delta\beta\mathcal{V}_{\text{inter}}}{\delta\rho_\alpha(\boldsymbol{r})} - \frac{v_\alpha}{v_s}\ln\left(1 - \sum_\alpha \rho_\alpha(\boldsymbol{r})v_\alpha\right). \tag{36}$$

The approach amounts to using an equation-of-state potential of the form

$$\beta\mathcal{V}_0\{\rho_\alpha\} = \frac{1}{v_s}\int \mathrm{d}\boldsymbol{r}\ (1-\eta(\boldsymbol{r}))\ln(1-\eta(\boldsymbol{r})) + \frac{1}{v_s}\int \mathrm{d}\boldsymbol{r}\ \eta(\boldsymbol{r}) \tag{37}$$

where the packing fraction $\eta(\boldsymbol{r}) = \sum_\alpha \rho_\alpha(\boldsymbol{r})v_\alpha$ is the local volume fraction occupied by monomers. The last term ensures that the free energy per monomer vanishes in the limit $\eta \to 0$. Equation (37) is a local version of the familiar compressible Flory–Huggins or Sanchez–Lacombe theory [70]. It provides an intuitive and straightforward treatment of compressibility effects in polymer blends. Unfortunately, the prediction for the equation of state of the melt can be rather poor [71], due to the total neglect of details of the monomer structure and local monomer correlations.

An alternative approach suggested in reference [72] conceives $\mathcal{V}_0$ as the density functional of a suitable reference system of identical monomers with no translational entropy. In the local density approximation, $\mathcal{V}_0$ can be derived from the equation of state $\Pi(\rho)$ ($\Pi$ is the pressure):

$$\beta\mathcal{V}_0 = \int \mathrm{d}\boldsymbol{r}\ \rho(\boldsymbol{r})f[\rho(\boldsymbol{r})] \qquad \text{with } f(\rho) = \int_0^\rho \mathrm{d}x\ \frac{\Pi(x)}{x^2}. \tag{38}$$

The function $f(\rho)$ is the local free energy per monomer. When studying interfaces or surfaces, $\mathcal{V}_0$ is conveniently replaced according to (20) by

$$\beta\tilde{\mathcal{V}}_0 = \int \mathrm{d}\boldsymbol{r}\ \left[\rho(\boldsymbol{r})(f[\rho(\boldsymbol{r})] - \omega^*) - \text{constant}\right] \tag{39}$$

where $\omega^* = f(\rho^*) + \rho^*(\mathrm{d}f/\mathrm{d}\rho)_{\rho^*}$ is the excess free energy per monomer at the bulk density $\rho^*$, and constant $= \rho^{*2}(\mathrm{d}f/\mathrm{d}\rho)_{\rho^*}$. The theory requires as input the knowledge of the equation of state of the reference system, i.e., a melt of infinitely long polymers built from the reference monomers. For example, one can take the Flory–Huggins form [25]

$$\Pi(\rho)/\rho = -1 - 1/\eta\ln(1-\eta) \tag{40}$$

with the packing fraction $\eta = \rho/\rho^*$, and recover the potential (37) with $v_s = 1/\rho^*$. On the basis of the Carnahan–Starling equation of state for single hard spheres, Dickman and Hall have derived an equation of state for hard chains [73], which compares well with computer simulations of hard chains, and even of the bond-fluctuation model [71]:

$$\Pi(\rho)/\rho = C_0\left[\frac{1+\eta+\eta^2-\eta^3}{(1-\eta)^3} - 1\right] \tag{41}$$

and leads to the free energy

$$f(\rho) = C_0\eta(4-3\eta)/(1-\eta)^2. \tag{42}$$

The constant $C_0$ depends on details of the intramolecular chain structure, and $\eta = a^3\rho\pi/6$ is the actual volume occupied by monomers of diameter $a$. Other forms for the equation of state are available as well [74]. In some cases, one may wish to include more information on the local liquid structure in the functional $\mathcal{V}_0$, and in the corresponding monomer excess free energy $\omega(\boldsymbol{r})$. Nath *et al* [75] suggest a modified version of the self-consistent-field theory, where the excess free energy is given by (cf. (19))

$$\tilde{\omega}(\boldsymbol{r}) = -\int \mathrm{d}\boldsymbol{r}'\ c(\boldsymbol{r}-\boldsymbol{r}')[\rho(\boldsymbol{r}) - \rho^*] + \omega^* \tag{43}$$

with the direct correlation functions $c(\boldsymbol{r})$ taken from P-RISM theory [38].

Next we discuss the second contribution $\mathcal{V}_{\text{inter}}$ to the free-energy functional $\mathcal{V}\{\rho_\alpha\}$, which describes the monomer-specific part of the interactions. Since it is small compared to the

total free energy of the system, we may assume a perturbative treatment. We split the pair interactions $W_{\alpha\beta}(\boldsymbol{r})$ between monomers $\alpha$ and $\beta$ into two parts:

$$W_{\alpha\beta}(\boldsymbol{r}) = W_0(\boldsymbol{r}) + W'_{\alpha\beta}(\boldsymbol{r}).$$

The potential $W_0(\boldsymbol{r})$ describes the interactions in the reference system $\mathcal{V}_0$. Then we define

$$\beta U_{\alpha\beta}(\boldsymbol{r}) = 1 - \exp[-\beta W'_{\alpha\beta}(\boldsymbol{r})]. \tag{44}$$

If $W'_{\alpha\beta}(\boldsymbol{r})$ is integrable and small, $U_{\alpha\beta}(\boldsymbol{r})$ reduces to $W'_{\alpha\beta}(\boldsymbol{r})$. More generally, the expression (44) also allows us to deal with effects of nonadditive packing, size disparities of monomers and the like (see also reference [44]). In perturbation theory [76], the free-energy contribution $\mathcal{V}_{\text{inter}}$ is given by

$$\mathcal{V}_{\text{inter}}\{\rho_\alpha\} = \frac{1}{2}\int \mathrm{d}\boldsymbol{r}\ \mathrm{d}\boldsymbol{r}'\ \sum_{\alpha\beta} U_{\alpha\beta}(\boldsymbol{r}-\boldsymbol{r}')\rho^{(2)}_{\alpha\beta}(\boldsymbol{r},\boldsymbol{r}'). \tag{45}$$

Here $\rho^{(2)}_{\alpha\beta}$ is the pair density of type-$\alpha$ monomers at $\boldsymbol{r}$ and type-$\beta$ monomers at $\boldsymbol{r}'$, which are *not* direct neighbours along one polymer chain. (The interactions between the latter contribute to the conformational weight functional $\mathcal{P}_j\{\boldsymbol{R}(\cdot)\}$.) Furthermore, the pair distribution function is approximated by

$$\rho^{(2)}_{\alpha\beta}(\boldsymbol{r},\boldsymbol{r}') = \rho_\alpha(\boldsymbol{r})\rho_\beta(\boldsymbol{r}')\gamma(\boldsymbol{r}-\boldsymbol{r}') \tag{46}$$

i.e., the monomer pair correlation function $\gamma(\boldsymbol{r})$ is taken to be independent of the identity of the interacting monomers, and of their densities [77].

If the interactions are short range, the profiles $\rho_\beta(\boldsymbol{r}')$ can be expanded around $\boldsymbol{r}$ [33]. With the definitions

$$\chi_{\alpha\beta} = \beta\rho^* \int \mathrm{d}\boldsymbol{r}\ U_{\alpha\beta}(\boldsymbol{r})\gamma(\boldsymbol{r}) \tag{47}$$

$$\sigma^{ij}_{\alpha\beta} = \beta\rho^* \int \mathrm{d}\boldsymbol{r}\ U_{\alpha\beta}(\boldsymbol{r})\gamma(\boldsymbol{r})r_i r_j \tag{48}$$

etc, one obtains

$$\beta\mathcal{V}_{\text{inter}}\{\rho_\alpha\} = \frac{1}{2\rho^*}\int \mathrm{d}\boldsymbol{r}\ \sum_{\alpha\beta}\left[\rho_\alpha(\boldsymbol{r})\rho_\beta(\boldsymbol{r})\chi_{\alpha\beta} - \frac{1}{2}\sum_{ij}\frac{\mathrm{d}\rho_\alpha}{\mathrm{d}r_i}\frac{\mathrm{d}\rho_\alpha}{\mathrm{d}r_j}\sigma^{ij}_{\alpha\beta} + \cdots\right]. \tag{49}$$

The indices $i$ run over cartesian coordinates $x$, $y$, $z$, and the bulk density $\rho^*$ was introduced in order to make $\chi_{\alpha\beta}$ dimensionless. The resulting excess potentials are given by

$$\omega_\alpha(\boldsymbol{r}) = \frac{\delta\beta\mathcal{V}_0}{\delta\rho} + \frac{1}{\rho^*}\sum_\beta\left[\chi_{\alpha\beta}\rho_\beta(\boldsymbol{r}) + \frac{1}{2}\sum_{ij}\sigma^{ij}_{\alpha\beta}\frac{\mathrm{d}^2\rho_\beta}{\mathrm{d}r_i\ \mathrm{d}r_j} + \cdots\right]. \tag{50}$$

In systems with only two types of monomer A and B, the parameters $\chi_{\alpha\beta}$ are usually combined to one single 'Flory–Huggins parameter'

$$\chi = \chi_{\text{AB}} - \frac{1}{2}(\chi_{\text{AA}} + \chi_{\text{BB}}). \tag{51}$$

Similarly, we define $\sigma^{ij} = \sigma^{ij}_{\text{AB}} - \frac{1}{2}(\sigma^{ij}_{\text{AA}} + \sigma^{ij}_{\text{BB}})$. The fields $\omega_{\text{A,B}}$ can then be rewritten as

$$\begin{aligned}
\omega_{\text{A}}(\boldsymbol{r}) &= \frac{\delta\beta\mathcal{V}_0}{\delta\rho} + \frac{1}{\rho^*}\chi\rho_{\text{B}} + \frac{1}{2\rho^*}\sum_{ij}\sigma^{ij}\frac{\mathrm{d}^2\rho_{\text{B}}}{\mathrm{d}r_i\ \mathrm{d}r_j} + h\{\rho(\boldsymbol{r})\} \\
\omega_{\text{B}}(\boldsymbol{r}) &= \frac{\delta\beta\mathcal{V}_0}{\delta\rho} + \frac{1}{\rho^*}\chi\rho_{\text{A}} + \frac{1}{2\rho^*}\sum_{ij}\sigma^{ij}\frac{\mathrm{d}^2\rho_{\text{A}}}{\mathrm{d}r_i\ \mathrm{d}r_j} - h\{\rho(\boldsymbol{r})\}
\end{aligned} \tag{52}$$

where

$$h\{\rho(\boldsymbol{r})\} = \frac{1}{4}(\chi_{AA} - \chi_{BB})\rho + \frac{1}{8}\sum_{ij}(\sigma^{ij}_{AA} - \sigma^{ij}_{BB})\frac{d^2\rho}{dr_i\ dr_j} \tag{53}$$

depends only on the total-density profile $\rho(\boldsymbol{r}) = \rho_A + \rho_B$, and contributions which are identical for both components have been dropped except for the leading term $\delta\beta\mathcal{V}_0/\delta\rho$. Similarly, the free-energy functional $\mathcal{V}_{inter}$ reads

$$\beta\mathcal{V}_{inter} = \frac{1}{\rho^*}\int d\boldsymbol{r}\left[\chi\rho_A\rho_B - \frac{1}{2}\sum_{ij}\sigma^{ij}\frac{d\rho_A}{dr_i}\frac{d\rho_B}{dr_j} + h\{\rho\}(\rho_A - \rho_B) + v\{\rho\}\right]. \tag{54}$$

Here again, $v\{\rho\}$ can be neglected compared to $\beta\mathcal{V}_0$.

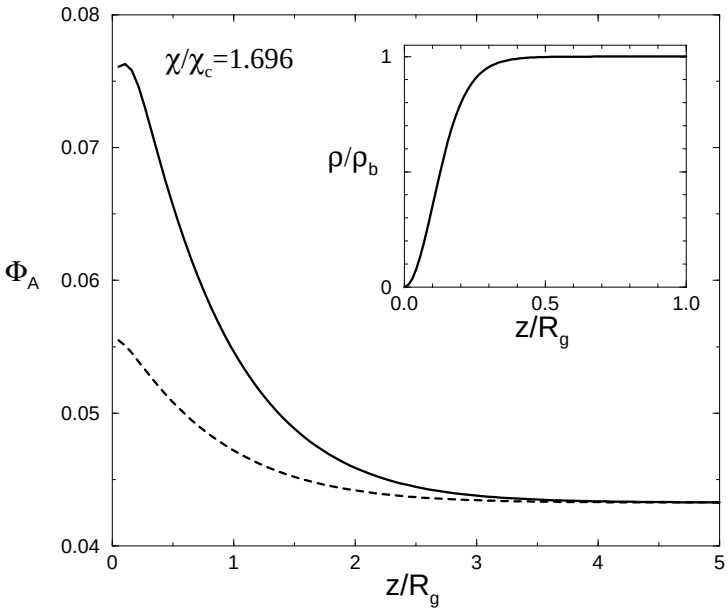


**Figure 1.** Surface segregation profiles of the minority component at coexistence below the demixing transition ($\chi_c$) in a symmetric polymer mixture. The dashed line shows the volume fraction profile for $\sigma = 0$, where the range of monomer interactions is assumed to be zero. The inset shows the total-density profile. From reference [72].

Usually, only the 'local' contributions ($\propto\chi_{\alpha\beta}$) are taken into account. However, the higher-order nonlocal terms become important in situations where the local density profiles vary strongly. We shall illustrate this using the example of surface segregation in a completely symmetric binary (A, B) blend of two incompatible, but otherwise identical homopolymers. Even if the surface is chosen neutral, i.e., the surface tensions of A and B are equal, the minority component segregates to the surface, because it has less unfavourable contacts with polymers of the majority component there. This effect is often called a 'missing-neighbour effect'. It increases with the range of the interactions, i.e., it should increase with the value of $\sigma$.

In reference [72], self-consistent-field calculations are presented for such a system. The parameters of the theory were adjusted to the bond-fluctuation model, a lattice model for polymers which has been widely used in Monte Carlo simulations and has extremely well-known bulk properties. It will be introduced in some more detail in section 3.2. The chain

conformations in the bulk [78], the equation of state [71, 79] and the thermodynamics of mixing [80] have been investigated in detail. Therefore, the model parameters for the self-consistent theory, e.g., within the Gaussian chain model, are all known. Figure 1 shows two segregation profiles at bulk two-phase coexistence, one with $\sigma = 0$ (dashed line) and one with $\sigma$ adapted to the bond-fluctuation model (solid line). (Note that the field $h\{\rho\}$, equation (53), which couples directly to the composition fluctuations, vanishes in a perfectly symmetric mixture.) In the limit of $\sigma = 0$ or pure contact interactions, surface segregation is almost entirely suppressed. Using the adjusted value of $\sigma$, one finds that the volume fraction $\Phi_A = \rho_A/\rho$ of the minority phase increases by almost a factor of two at the surface.

The self-consistent-field results can be compared with the Monte Carlo simulations of Rouault *et al* [81]. Figure 2 shows the predicted difference between the volume fractions of A at the surface and in the bulk $\Delta\Phi_A$, and corresponding Monte Carlo data. The simulations were performed in a slab geometry with a slab thickness of about three times the gyration radius of the chains. In such a thin film, the composition variable $|\rho_A - \rho_B|$ at coexistence is reduced compared to that of the bulk system. The difference between the volume fraction $\Phi_A$ at the surface of the thin film and in the bulk of the infinite system thus gives an upper bound for the actual value of $\Delta\Phi_A$. The difference between $\Phi_A$ at the surface and in the centre of the thin film gives a lower bound. Figure 2 illustrates that the theoretical prediction lies nicely within these two bounds. We emphasize that the good agreement was reached without using any adjustable parameters. However, the range of the monomer interactions has to be accounted for correctly, i.e., the nonlocal term $\sigma$ may not be neglected in this situation with strong density variations.

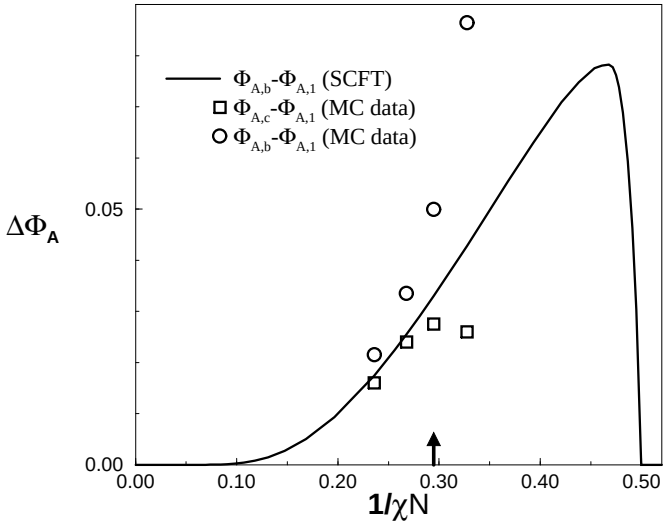


**Figure 2.** The difference $\Delta\Phi_A$ between the volume fraction of the minority component at the surface and in the bulk, at two-phase coexistence, versus $1/\chi N$ ($N = 32$). Data points show the simulation results of Rouault *et al* (reference [81]): the upper bound for $\Delta\Phi_A$ (circles), and the lower bound (squares). The arrow indicates the value of $1/\chi N$ which corresponds to figure 1. From reference [72].

A second caveat applies to the approximation (46). In general, the pair correlation function depends on the identity of the monomers, and on the local environment. For example, the number of monomer contacts divided by the local density typically decreases in the vicinity of an interface [82], and is different for homopolymers and copolymers [83].

This is a higher-order effect in our perturbative approach, which is usually not taken into account in self-consistent-field theories. Maurer *et al* have recently found experimental evidence that it may engender a difference of the effective $\chi$-parameter in homopolymer and block-copolymer blends [84].

### *2.4. Fluctuations*

In the limit of infinite chain length (while keeping the densities constant), the saddle-point integrations leading to the free-energy expression (16) become exact. At any finite chain length, however, the free energy is affected by concentration fluctuations. On the one hand, the concentrations always fluctuate locally about their local mean value. The length scale for these fluctuations is given by the bulk correlation length, which is usually roughly the gyration radius and diverges only very close to a critical point. In systems with interfaces, a second qualitatively different type of fluctuation emerges: since the interface breaks a continuous symmetry—the translational symmetry—long-wavelength Goldstone excitations come into existence which cost virtually no energy in the zero-wavelength limit. The corresponding length scale thus diverges at all temperatures. These fluctuations are sometimes referred to as interface 'waviness', or capillary-wave fluctuations.

Local concentration fluctuations can be assessed systematically using an expansion of local concentration perturbations:

$$\delta\rho_\alpha(\boldsymbol{r}) = \rho_\alpha(\boldsymbol{r}) - \rho_\alpha^{SCF}(\boldsymbol{r})$$

about the SCF concentration profiles $\rho_\alpha^{SCF}(\boldsymbol{r})$. A way to perform such a perturbative extension of the self-consistent-field theory has recently been suggested for incompressible mixtures in the canonical ensemble by Shi, Noolandi and Desai [53]. In the following, we shall briefly sketch their approach, and generalize it for the case of compressible mixtures and arbitrary statistical ensemble. Capillary-wave fluctuations will be discussed subsequently.

The starting point is the partition function (11) or (15). In the perturbative treatment, the free-energy functional $\mathcal{F}\{\rho_\alpha, \omega_\alpha\{\rho_\alpha\}\}$ is expanded about its self-consistent-field minimum $F^{SCF}$. Following Shi *et al*, this is done most conveniently by expanding $\mathcal{F}_C\{\rho_\alpha, \omega_\alpha\}$ in both $\delta\rho_\alpha$ and the field deviations $\delta\omega_\alpha = \omega_\alpha\{\rho_\alpha\} - \omega_\alpha\{\rho_\alpha^{SCF}\}$, keeping in mind that the latter are functions of the concentration perturbations $\delta\rho_\alpha$. It is useful to define the single-chain $k$-point distribution function

$$g^j_{\alpha_1\cdots\alpha_k}(\boldsymbol{r}_1\cdots\boldsymbol{r}_k) = \frac{1}{\mathcal{Q}_j}\frac{\delta^k\mathcal{Q}_j}{\delta\omega_{\alpha_1}(\boldsymbol{r}_1)\cdots\delta\omega_{\alpha_k}(\boldsymbol{r}_k)} \tag{55}$$

which is the joint $k$-point density $\langle\widehat{\rho}^j_{\alpha_1}(\boldsymbol{r}_1)\cdots\widehat{\rho}^j_{\alpha_k}(\boldsymbol{r}_k)\rangle$ for monomers of the same chain of type $j$. The corresponding cumulant correlation functions are given by

$$c^j_{\alpha_1\cdots\alpha_k}(\boldsymbol{r}_1\cdots\boldsymbol{r}_k) = \frac{\delta^k\ln\mathcal{Q}_j}{\delta\omega_{\alpha_1}(\boldsymbol{r}_1)\cdots\delta\omega_{\alpha_k}(\boldsymbol{r}_k)}. \tag{56}$$

For example, the lowest cumulant correlation function is simply the density, $c^j_\alpha(\boldsymbol{r}) = g^j_\alpha(\boldsymbol{r}) = \langle\widehat{\rho}^j_\alpha\rangle$, the pair correlation function is

$$c^j_{\alpha\beta}(\boldsymbol{r},\boldsymbol{r}') = \langle\widehat{\rho}^j_\alpha(\boldsymbol{r})\widehat{\rho}^j_\beta(\boldsymbol{r}')\rangle - \langle\widehat{\rho}^j_\alpha(\boldsymbol{r})\rangle\langle\widehat{\rho}^j_\beta(\boldsymbol{r}')\rangle$$

etc. Note that these are single-chain correlation functions of noninteracting chains $j$ subject to the external fields $\omega_\alpha(\boldsymbol{r})$. For convenience, we also introduce the notation

$$\mathcal{V}^{(k)}_{\alpha_1\cdots\alpha_k}(\boldsymbol{r}_1\cdots\boldsymbol{r}_k) = \left.\frac{\delta^k\mathcal{V}}{\delta\rho_{\alpha_1}(\boldsymbol{r}_1)\cdots\delta\rho_{\alpha_k}(\boldsymbol{r}_k)}\right|_{\{\rho_\alpha^{SCF}\}} \tag{57}$$

and define the functions $K_{\alpha_1\cdots\alpha_k}(\boldsymbol{r}_1\cdots\boldsymbol{r}_k)$:

$$K_{\alpha_1\cdots\alpha_k}(\boldsymbol{r}_1\cdots\boldsymbol{r}_k) = \begin{cases} \sum_j n_j c^j_{\alpha_1\cdots\alpha_k}(\boldsymbol{r}_1\cdots\boldsymbol{r}_k) & \text{(canonical ensemble)} \\ \sum_j \exp(\beta\mu_j)\mathcal{Q}_j g^j_{\alpha_1\cdots\alpha_k}(\boldsymbol{r}_1\cdots\boldsymbol{r}_k) & \text{(grand canonical ensemble).} \end{cases} \tag{58}$$

With these definitions, and using equations (10), (14), and (17), the free-energy functional (8) or (13) can be expanded as

$$\begin{aligned}\beta\mathcal{F}\{\rho_\alpha,\omega_\alpha\} = \beta F^{SCF} &- \sum_\alpha \int \mathrm{d}\boldsymbol{r}\ \delta\rho_\alpha(\boldsymbol{r})\,\delta\omega_\beta(\boldsymbol{r}') \\ &+ \sum_{k=2}^{\infty}\frac{1}{k!}\sum_{\alpha_1\cdots\alpha_k}\int \mathrm{d}\boldsymbol{r}_1\ \cdots\ \mathrm{d}\boldsymbol{r}_k\ \Big\{\beta\mathcal{V}^{(k)}_{\alpha_1\cdots\alpha_k}(\boldsymbol{r}_1\cdots\boldsymbol{r}_k)\,\delta\rho_{\alpha_1}(\boldsymbol{r}_1)\ \cdots\ \delta\rho_{\alpha_k}(\boldsymbol{r}_k) \\ &- K_{\alpha_1\cdots\alpha_k}(\boldsymbol{r}_1\cdots\boldsymbol{r}_k)\,\delta\omega_{\alpha_1}(\boldsymbol{r}_1)\ \cdots\ \delta\omega_{\alpha_k}(\boldsymbol{r}_k)\Big\}.\end{aligned} \tag{59}$$

The field deviations $\delta\omega_\alpha$ are functions of the concentration perturbations by means of the relation (10) in the canonical ensemble, or the relation (14) in the grand canonical ensemble. In terms of the correlation functions $K$ introduced above, these can be rewritten as

$$\delta\rho_\alpha(\boldsymbol{r}) = -\sum_{k=2}^{\infty}\frac{1}{(k-1)!}\sum_{\alpha_2\cdots\alpha_k}\int \mathrm{d}\boldsymbol{r}_2\ \cdots\ \mathrm{d}\boldsymbol{r}_k\ K_{\alpha\alpha_2\cdots\alpha_k}(\boldsymbol{r}\boldsymbol{r}_2\cdots\boldsymbol{r}_k)\,\delta\omega_{\alpha_2}(\boldsymbol{r}_2)\ \cdots\ \delta\omega_{\alpha_k}(\boldsymbol{r}_k). \tag{60}$$

To leading order in $\delta\rho_\alpha$, one gets

$$\delta\omega_\alpha(\boldsymbol{r}) = -\sum_\beta \int \mathrm{d}\boldsymbol{r}'\ K^{-1}_{\alpha\beta}(\boldsymbol{r},\boldsymbol{r}')\,\delta\rho_\beta(\boldsymbol{r}'), \tag{61}$$

where $K^{-1}_{\alpha\beta}$ is the inverse of $K_{\alpha\beta}$, defined through the relation

$$\sum_\gamma \int \mathrm{d}\boldsymbol{r}''\ K^{-1}_{\alpha\gamma}(\boldsymbol{r},\boldsymbol{r}'')K_{\gamma\beta}(\boldsymbol{r}'',\boldsymbol{r}') = \delta_{\alpha\beta}\,\delta(\boldsymbol{r}-\boldsymbol{r}').$$

Inserting this into equation (59) yields the Gaussian contribution of the fluctuations to the free-energy functional:

$$\beta\mathcal{F} = \beta F^{SCF} + \frac{1}{2}\sum_{\alpha\beta}\int \mathrm{d}\boldsymbol{r}\ \mathrm{d}\boldsymbol{r}'\ \{\beta\mathcal{V}^{(2)}_{\alpha\beta}(\boldsymbol{r},\boldsymbol{r}') + K^{-1}_{\alpha\beta}(\boldsymbol{r},\boldsymbol{r}')\}\,\delta\rho_\alpha(\boldsymbol{r})\,\delta\rho_\beta(\boldsymbol{r}') + \cdots. \tag{62}$$

The study of these harmonic fluctuations already permits a stability analysis of the self-consistent-field solution $F^{SCF}$, and the calculation of scattering functions. The partition function in leading harmonic order contains only Gaussian integrals and can be evaluated in a straightforward way. At first sight, inverting the function $K_{\alpha\beta}(\boldsymbol{r},\boldsymbol{r}')$ seems a difficult task. However, a considerable simplification can often be achieved by an appropriate basis transformation, i.e., expressing $K_{\alpha\beta}$, $\rho_\alpha$ etc in terms of suitable basis functions—for example, in periodically ordered structures an expansion in the Bloch waves belonging to the periodically ordered potential $\omega_\alpha(\boldsymbol{r})$ has proved useful [53]. Higher-order corrections to equation (62) can be obtained iteratively, yet their treatment becomes much more involved.

It is often expedient to recast the theory in a way which allows one to separate total-density fluctuations from composition fluctuations. For simplicity, we shall now consider a mixture which contains only two types of monomer, A and B, of equal size. We replace the variables $(\rho_A, \rho_B)$ by $(\rho, \phi)$ with the total density $\rho = \rho_A + \rho_B$, and the composition variable $\phi = \rho_A - \rho_B$. The conjugate fields are given by $\omega_\rho = (\omega_A + \omega_B)/2$ and $\omega_\phi = (\omega_A - \omega_B)/2$. Furthermore, we adopt the definitions of Laradji *et al* [54]:

$$\begin{aligned} \Sigma &= K_{AA} + K_{AB} + K_{BA} + K_{BB} \\ \Delta_1 &= K_{AA} + K_{AB} - K_{BA} - K_{BB} \\ \Delta_2 &= K_{AA} - K_{AB} + K_{BA} - K_{BB} \\ C &= K_{AA} - K_{AB} - K_{BA} + K_{BB} \end{aligned} \tag{63}$$

and adopt the matrix notation

$$\Sigma \delta\omega_\rho = \int \mathrm{d}\boldsymbol{r}' \; \Sigma(\boldsymbol{r}, \boldsymbol{r}')\, \delta\omega_\rho(\boldsymbol{r}').$$

Equation (60) can then be rewritten to leading Gaussian order as

$$\begin{pmatrix} \delta\rho \\ \delta\phi \end{pmatrix} = \begin{pmatrix} \Sigma & \Delta_2 \\ \Delta_1 & C \end{pmatrix} \begin{pmatrix} \delta\omega_\rho \\ \delta\omega_\phi \end{pmatrix} + \cdots. \tag{64}$$

Inverting this expression yields

$$\begin{pmatrix} \delta\omega_\rho \\ \delta\omega_\phi \end{pmatrix} = \begin{pmatrix} \tilde{\Sigma}^{-1} & \tilde{\Delta}_1^{-1} \\ \tilde{\Delta}_2^{-1} & \tilde{C}^{-1} \end{pmatrix} \begin{pmatrix} \delta\rho \\ \delta\phi \end{pmatrix} + \cdots \tag{65}$$

with

$$\begin{aligned} \tilde{\Sigma} &= \Sigma - \Delta_2 C^{-1} \Delta_1 \\ \tilde{\Delta}_1 &= \Delta_1 - C\Delta_2^{-1}\Sigma \\ \tilde{\Delta}_2 &= \Delta_2 - \Sigma\Delta_1^{-1} C \\ \tilde{C} &= C - \Delta_1 \Sigma^{-1} \Delta_2. \end{aligned} \tag{66}$$

The free-energy expansion (62) thus takes the form

$$\beta\mathcal{F} = \beta F^{SCF} + \frac{1}{2}(\delta\rho \;\; \delta\phi) \begin{pmatrix} \tilde{\Sigma}^{-1} + \beta\mathcal{V}^{(2)}_{\rho\rho} & \tilde{\Delta}_1^{-1} + \beta\mathcal{V}^{(2)}_{\rho\phi} \\ \tilde{\Delta}_2^{-1} + \beta\mathcal{V}^{(2)}_{\phi\rho} & \tilde{C}^{-1} + \beta\mathcal{V}^{(2)}_{\phi\phi} \end{pmatrix} \begin{pmatrix} \delta\rho \\ \delta\phi \end{pmatrix} + \cdots \tag{67}$$

where $\mathcal{V}^{(2)}_{\phi\phi}(\boldsymbol{r}, \boldsymbol{r}')$ is defined as $\delta^2\mathcal{V}/\delta\phi(\boldsymbol{r})\,\delta\phi(\boldsymbol{r}')$ etc, in analogy to equation (57). Usually, in the literature [53–55], incompressible melts have been considered ($\delta\rho = 0$) with an interaction potential of the form

$$\beta\mathcal{V}_{\text{inter}} = \int \mathrm{d}\boldsymbol{r} \; \chi(\rho_A\rho_B)/\rho.$$

In this case, the free energy can be written as

$$\beta\mathcal{F} = \beta F^{SCF} + \frac{1}{2}\,\delta\rho\,[C^{RPA}]^{-1}\,\delta\rho \qquad \text{with } C^{RPA} = \left[\tilde{C}^{-1} - \frac{\chi}{2}\mathbf{1}\right]^{-1}. \tag{68}$$

Equation (67) generalizes this result for arbitrary potentials $\mathcal{V}$ and compressible blends.

In well-segregated macro- or microseparated blends, the main composition fluctuations are due to capillary-wave fluctuations of interface positions. These are less well captured by perturbative treatments, since the local concentration deviations $\delta\rho_\alpha(\boldsymbol{r})$ are not small. As long as the interfaces are still localized, i.e., in periodic structures, the method can still be applied to some extent [53]. However, the expansion will fail if the fluctuations

are strong enough to destroy the long-range order. Note that single, isolated interfaces between macroscopic phases usually delocalize [85–89], i.e., the extent of the fluctuations depends on the size of the system. In order to study these long-wavelength fluctuations, other approaches like effective-interface descriptions with input parameters taken from self-consistent-field calculations are more appropriate.

In order to illustrate the problem, we shall discuss the simplest example, a single interface separating two macroscopic phases in a blend of incompatible, but otherwise symmetric A and B homopolymers. Let us assume that is only slightly distorted from its lowest-energy flat state, such that the local deviations of the interfacial position can be described by a single-valued function $h(x, y)$, and the gradients $|\nabla h|$ are small. The increase in interfacial area caused by these fluctuations cost the free energy

$$\mathcal{H}_{CW} = \frac{\sigma}{2} \int \mathrm{d}x \ \mathrm{d}y \ |\nabla h|^2 \tag{69}$$

where $\sigma$ is the interfacial tension, and energy losses due to the distortion of profiles and the like have been neglected. The functional (69) is commonly referred to as the capillary-wave Hamiltonian. It can be diagonalized by means of a Fourier transformation in $x$ and $y$, and since it is quadratic, the spectrum and the distribution functions can be determined analytically. The thermal average of the Fourier components is given by $\langle |h(\boldsymbol{q})|^2 \rangle = k_B T/(\sigma q^2)$ and one obtains a Gaussian height distribution function [85]

$$\langle \delta(z - h(x, y)) \rangle = P_{s^2}(z) = \frac{1}{2\pi s^2} \exp\left(-\frac{z^2}{2s^2}\right) \tag{70}$$

with

$$s^2 = \frac{1}{4\pi^2} \int \mathrm{d}\boldsymbol{q} \ \langle |h(\boldsymbol{q})|^2 \rangle = \frac{1}{2\pi\sigma} \ln\left(\frac{q_{\max}}{q_{\min}}\right). \tag{71}$$

Here one has to introduce an upper cut-off $q_{\max}$ and a lower cut-off $q_{\min}$, since the integral $\int \mathrm{d}q/q$ diverges both at $q \to \infty$ and $q \to 0$. The lower cut-off is obviously given by the system size, $q_{\min} = 2\pi/L$. An important consequence is that the width $s$ of the distribution function $P(h)$ grows logarithmically with the system size $L$, i.e., the interface is marginally rough.

The value of the upper cut-off is less obvious. Clearly, the capillary-wave Hamiltonian (69) cannot be expected to provide a good description of polymer interfaces on all length scales. Ideally, one would hope that one can find a microscopic length $1/q_{\max}$ beyond which (69) is valid, and that the system can be studied independently by other means on smaller length scales. This implies that the coupling of the long-wavelength capillary-wave fluctuations with the local structure on short length scales can be neglected. In that case, an approximation makes sense which describes the interfacial structure in terms of local 'intrinsic' profiles, centred at the local interface position, $\rho_\alpha(x, y, z) = \rho_\alpha^{(int)}(z - h(x, y))$ (the convolution approximation [90]). The intrinsic profile characterizes the system on the length scale of $1/q_{\max}$. When looking at the interface on a larger length scale $1/q_0$, one obtains apparent profiles $\rho_\alpha^{(app)}(z)$, which are broadened by the capillary-wave modes with wavevectors between $q_0$ and $q_{\max}$:

$$\rho_\alpha^{(app)}(z) = \int_{-\infty}^{\infty} \mathrm{d}h \ \rho_\alpha^{(int)}(z - h) P_{s'^2}(h) \qquad \text{with } s'^2 = \frac{1}{2\pi\sigma} \ln(q_{\max}/q_0). \tag{72}$$

Note that since

$$P_{s^2}(z) = \int_{-\infty}^{\infty} \mathrm{d}h \ P_{s'^2}(z - h) P_{(s^2 - s'^2)}(h)$$

the intrinsic profile $\rho_\alpha^{(int)}(z)$ can be replaced by $\rho_\alpha^{(app)}(z)$, and the upper cut-off $q_{\max}$ by $q_0$, without affecting anything on length scales beyond $1/q_0$. Thus the choice of the upper cut-off is largely arbitrary.

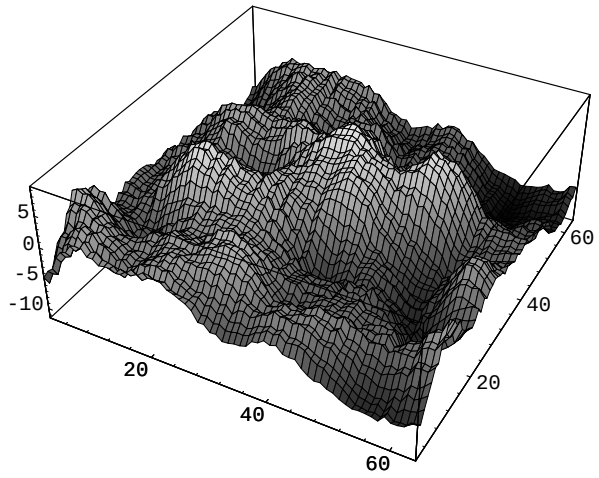


**Figure 3.** A typical snapshot picture of the local interface position $h(x, y)$ in Monte Carlo simulations of a symmetric homopolymer interface at $\chi = 0.16$, $N = 32$. The coarse-graining length $B = 8$ is roughly the chain's gyration radius. The system dimensions are $D = 64$ and $L = 64$. From reference [91].

Werner *et al* [91] have tested this concept by carrying out extensive Monte Carlo simulations of interfaces between immiscible phases in symmetric binary polymer blends, within the bond-fluctuation model (see section 3.1). The simulations were done in a $L \times L \times D$ geometry with periodic boundary conditions in the $L$-directions, and hard walls in the $D$-direction, one of which favours the A component while the other favours the B component. The wall interaction parameters were chosen to be beyond the wetting transition, and hence large enough to enforce a delocalized AB interface which is on average located in the middle of the film. In thin films, the capillary-wave fluctuations are limited by the film thickness $D$ rather than by the system size $L$. However, if the film thickness $D$ is chosen large enough compared to $L$, the interface is essentially free. In order to study the interfacial fluctuations, the system was split into columns of block size $B \times B$ and height $D$, and the Gibbs dividing surface $h(x, y)$ was determined in each column. A typical snapshot of the resulting local interface position $h(x, y)$ is shown in figure 3 for the block size $B = 8$ lattice constants, which is roughly the radius of gyration ($R_g \approx 7.05$). The monomer profiles were then taken relative to this position, and after averaging over all columns, the interfacial width $w$ was determined by fitting the order parameter profile $m(z) = (\rho_{\mathrm{A}}(z) - \rho_{\mathrm{B}}(z))/\rho(z)$ to a tanh profile, $m(z) = m_b \tanh(z/w)$. Using equation (72), one can show [91] that the apparent width obtained with this procedure is broadened according to

$$w^2 = w_0^2 + \frac{1}{4\sigma} \ln\left(\frac{B}{B_0}\right) \tag{73}$$

due to capillary waves, where $w_0$ is the intrinsic width and $B_0 = 2\pi/q_{\max}$ is the coarse-graining length associated with the upper cut-off $q_{\max}$. Figure 4 shows the simulation results for the squared interfacial width $w^2$ as a function of block size $B$ in films of lateral size

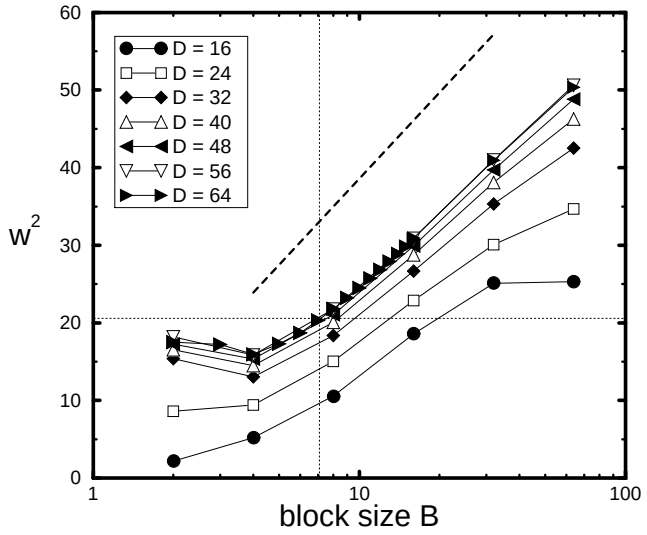


**Figure 4.** The squared interfacial width $w^2$ as a function of the block size $B$ in Monte Carlo simulations of a homopolymer interface confined in films of various thicknesses $D$ with lateral dimension $L = 128$, at $\chi = 0.16$ and $N = 32$. The horizontal dotted line marks the self-consistent-field prediction for a free interface $w^2 = 20.5$, and the vertical dotted line the value of the gyration radius of a chain $R_g = 7.05$. The dashed line indicates the theoretically predicted slope of $1/(4\sigma)\ln(B)$, with $\sigma = 0.0156$ taken from the self-consistent-field theory. From reference [91].

$L = 128$, for various film thicknesses $D$. They become independent of $D$ for thicknesses larger than $D > 48$, and hence the interface can then be considered to be free. For large block sizes $B$, $w^2$ grows logarithmically with $B$, with a slope which is in rough agreement with the theoretical prediction $1/(4\sigma)$ (dashed line). For very small block sizes $B \leqslant 4$, $w^2$ becomes flat. The self-consistent-field value $w^2_{SCF} = 20.9$ is reached at the block size $B_0 \approx 7$. However, looking just at figure 4, nothing in the shape of the curves indicates that there should be anything special about the block size 7 or about $w^2 = 20.5$. The regime of logarithmic growth starts at much smaller block sizes. On the other hand $w_{SCF}$ can be made the intrinsic width by decree. With the upper cut-off $q_{\max}$ defined by the corresponding block size $B_0$, the capillary-wave Hamiltonian then provides a reasonable description of the simulation data. The question remains of which is the correct choice of the cut-off $B_0$. In our example, $B_0$ happens to be exactly the gyration radius of the chain, but also twice the statistical segment length of a chain ($b = 3.05$), or one and a half times the interfacial width. Each of these is a valid candidate for the cut-off parameter. Semenov [87], for example, favours the interfacial width. Here again simulations can help to clarify the issue. Recently, Werner *et al* have repeated the analysis leading to figure 4 with systematically varied chain length $N$ and/or monomer interaction, i.e., $\chi$-parameter. At fixed $\chi N = 0.51$, they find that the cut-off $B_0$, defined by $w(B_0) = w_{SCF}$, scales like $B_0 \propto \sqrt{N} \propto \sqrt{1/\chi} \propto w_{SSL} \propto R_g$. At fixed $\chi = 0.16$, $B_0$ first increases strongly with $N$, but levels off faster than $R_g \propto \sqrt{N}$ at the largest chain lengths ($N = 256$) [92, 93].

In order to gain a better understanding of this problem, let us go back to the case of infinitely long chains and recall that self-consistent-field theory is supposed to be exact in this limit. More specifically, it gives the correct free energy of the system. On the other hand, the interface has a given, finite surface tension (e.g., $\sigma_{SSL}$ as obtained in [32]),

and hence the interface position will fluctuate. Concentration fluctuations may exist in the long-chain limit; they just do not affect the thermodynamics of the system. However, they influence the local structure, such as local concentration profiles or orientational properties at interfaces. Self-consistent-field calculations can thus not be expected to give equally good results on all length scales. When they are used to study local structure properties in polymer mixtures, one has to ask which is the length scale where the theories describe the system best. The simulations of Werner *et al* suggest that it probably approaches a constant ($B_0 \rightarrow (4\text{–}5)w_{SSL}$) in the strong-segregation limit, but is subject to strong chain-end corrections. It is worth noting that the cut-off $B_0$ is always much larger than the block size at which $w(B)^2$ starts to grow logarithmically as predicted by (73). Up to the length scale of $B_0$, the structures obtained with self-consistent-field theories thus average not only over the bulk composition fluctuations, but also over the capillary-wave fluctuations of the interface position.

## 3. Applications

Self-consistent-field theories are finding widespread use in numerous contexts of polymer and macromolecular physics. For example, they have been employed to calculate complicated phase diagrams of copolymer blends or mixtures of copolymers and homopolymers [61, 94], and to study details of density profiles at the internal interfaces in such materials [35, 86, 95–97]. They are frequently applied in surface physics, e.g., in connection with surface segregation [98, 69, 72] and wetting phenomena [99], and for the theoretical study of polymers or copolymers which are adsorbed on surfaces or grafted to surfaces [40, 100, 101]. We shall not attempt to give an account of all of these activities here. Rather, we refer the reader to the various recent reviews on the different topics, e.g., references [40, 51, 61, 102], and illustrate the use of the method with two examples which are taken from the present author's own research: a comparison between self-consistent-field calculations and Monte Carlo simulations of polymer conformations at interfaces, and a self-consistent-field study of the phase behaviour of short amphiphilic molecules at surfaces.

### *3.1. Conformations of polymers at interfaces*

We consider an interface between coexisting phases in a symmetric mixture of homopolymers A and B, in the strong-segregation regime ($\chi N = 17$), i.e., at temperatures well below the demixing temperature. It is studied by means of self-consistent-field theory within the Gaussian chain model and the wormlike chain model.

The self-consistent-field calculations are compared with simulations of the bond-fluctuation model. The latter represents polymers by chains of spatially extended effective monomers, which each occupy a cube of eight neighbouring sites on a cubic lattice, and which are connected by bonds of length $\leqslant\sqrt{10}$ lattice spacings. The two types of monomer A and B interact pairwise, with interactions $\epsilon_{AA} = \epsilon_{BB} = -\epsilon_{AB} = -k_B T\epsilon$, if they are less than $\sqrt{6}$ lattice units apart. The equation of state and the local pair correlations in the bulk are well known. Moreover, the model was shown to behave like a dense melt at volume fraction 0.5 or density $\rho = 1/16$, i.e., the chains have almost ideal Gaussian statistics, with known statistical segment length $b \approx 3$ lattice units. The simulations were performed at chain length $N = 32$ and interaction strength $\epsilon = 0.1$, which corresponds to $\chi = 0.53$.

Figure 5 shows the results for the interfacial profile ([62] and [92]). All lengths are given in units of $w_{SSL} = b/\sqrt{6\chi}$, which is the interfacial width in an incompressible mixture of infinitely long polymers [32], and a 'natural' unit of length within the self-consistent-

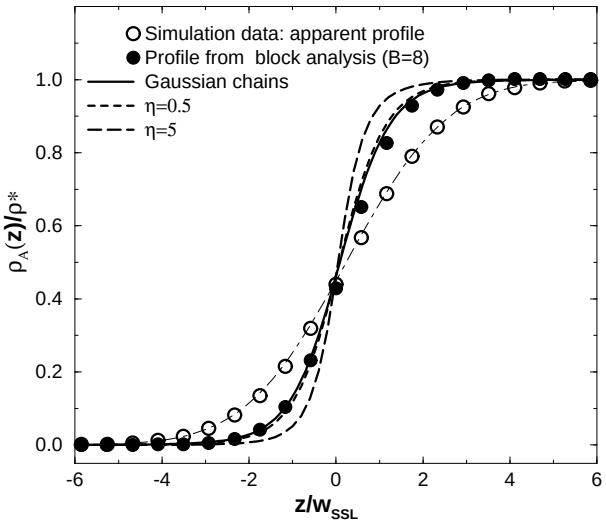


**Figure 5.** The concentration profile $\rho_A/\rho^*$ versus $z/w_{SSL}$ (with $w_{SSL} = b/\sqrt{6\chi}$) in self-consistent-field theory for Gaussian chains (solid line) and wormlike chains of different chain stiffness $\eta$ (dashed lines), at $\chi = 0.53$ and chain length $N = 32$. The results are compared to simulation data without (open circles) and with (closed circles) block splitting. The thin dashed–dotted line shows the profile for $\eta = 0.5$ with capillary-wave correction, assuming $s^2 = 2.5$ (see equation (72)) (reference [103]). From references [62] and [92].

field theory. In these units, the self-consistent-field theory predicts that the interfacial thickness decreases with increasing chain stiffness $\eta$. However, the statistical segment length $b = a\sqrt{2\eta}$ increases in turn, such that the net effect is positive: in absolute units (e.g., units of the monomer size $a$), the interfacial width increases with the chain stiffness $\eta$ in this regime of relatively small chain stiffness $\eta$. (Note that Morse and Fredrickson predict the opposite effect, a decrease of the interfacial width, in the limit of large $\eta$ [49].)

We turn to the comparison with the Monte Carlo data. The normalization in units of $w_{SSL}$ still makes sense, since $b$ and $w_{SSL}$ are known, whereas the parameter $\eta$ is not. The bare simulation profile is broader by a factor of almost two than the self-consistent-field prediction (open circles). However, this can basically be traced back to the effect of capillary waves, as discussed in section 2.4. The simulation profiles obtained after splitting the system into blocks of size $B = 8 \approx R_g$ as in reference [91] (where the much more weakly segregated case $\chi = 0.16$ was studied) are in good agreement with the self-consistent-field prediction (closed circles) [62]. Alternatively, one can also correct the self-consistent-field profile for capillary-wave broadening by means of equation (72) (reference [103]).

Next, the conformations of polymers in the vicinity of such an interface are analysed. We will examine the conformations of the constituent homopolymers, and those of single symmetric A:B diblock copolymers (of the same length), which adsorb to the interface. The results can again be compared with Monte Carlo simulations of very diluted copolymers at a homopolymer interface [83]. We will limit ourselves to the discussion of the orientational properties of the molecules here.

It is instructive to study separately the orientations of single bonds, of chain segments, and of whole chains. In self-consistent-field theory, bond orientations are conveniently calculated within the wormlike chain model. In the following, we will set $\eta = 1/2$. At that stiffness, the statistical segment length $b$ is identical to the 'monomer length' $a$, and hence

adjacent monomers are essentially uncorrelated. This assumption seems reasonable for the bond-fluctuation model, as long as no bond potentials have been introduced. (An improved guess for $\eta$ would probably be a value slightly larger than $1/2$, since chains cannot fold back onto themselves.) Note that chains with such a small stiffness behave almost like Gaussian chains (cf., e.g., figure 5).

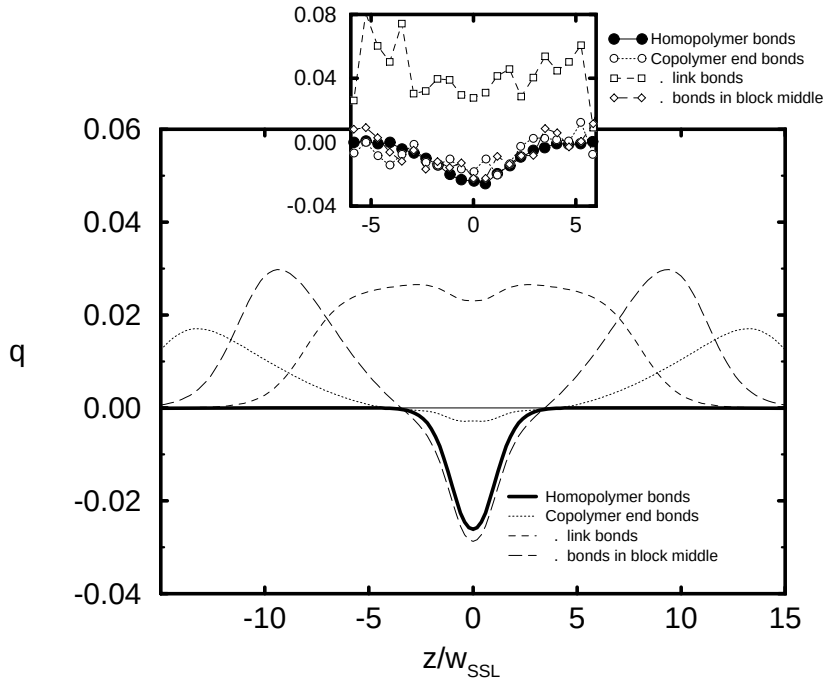


**Figure 6.** The orientational order parameter $q$ versus $z/w_{SSL}$ at a homopolymer interface ($\chi = 0.53$, $N = 32$) for homopolymer bonds (thick solid line) and for bonds in an adsorbed diblock copolymer at different positions within the chain: end bonds (dotted line), bonds linking the two blocks (dashed line), bonds in the middle of a block (long-dashed line). The inset shows corresponding Monte Carlo data. From references [62] and [83].

In order to study profiles of the bond orientations $\boldsymbol{b}$, we define the bond-orientation parameter

$$q(\boldsymbol{r}) = \frac{\langle b_z^2\rangle - \frac{1}{2}(\langle b_x^2\rangle + \langle b_y^2\rangle)}{\langle \boldsymbol{b}^2\rangle} \tag{74}$$

which is negative for orientation parallel to the interface, and positive for perpendicular orientation. The interfacial profiles of $q$ are shown in figure 6. Orientation effects on the bond level are found to be overall very weak. Homopolymer bonds tend to orient parallel to the interface in the interfacial region. The same holds for most parts of the copolymer; only very few bonds in the central region connecting the A and B block are perpendicular to the interface. For both copolymers (dotted line) and homopolymers (not shown), the orientation is weakest at the chain ends. These results are basically in agreement with the Monte Carlo data (inset) [83].

Further away from the interface, the orientation of copolymer monomers is driven by a different effect. The chains are pulled towards the interface by one copolymer end, and the bonds align perpendicularly as a result. At distances of several radii of gyration, the

copolymers lose contact with the interface and the orientation parameter $q$ drops back to zero. The profile of $q$ for copolymers thus reflects two different length scales—a tendency of parallel alignment in a region of the extent of the interfacial width, which gives rise to the central dip in the profiles, and a force towards perpendicular alignment over the length scale of the gyration radius, which is the range of the interaction between the copolymer and the interface. Note however that most copolymer monomers are located close to the centre of the interface, and the net bond orientation is parallel.

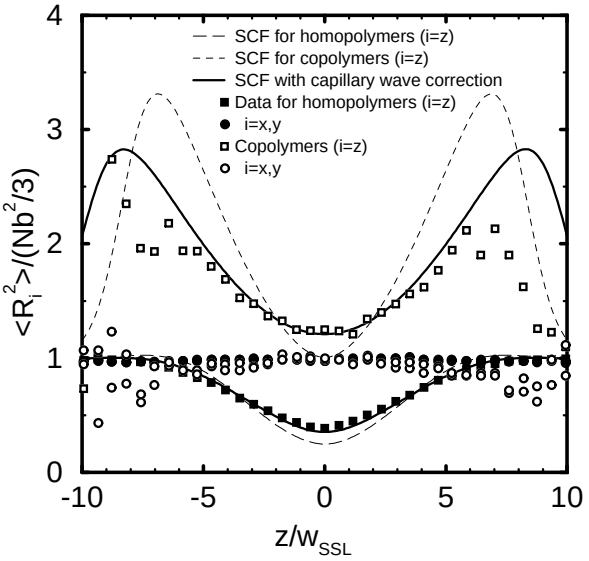


**Figure 7.** The mean square end-to-end vector component $\langle R_i^2 \rangle$ for $i = x, y, z$ in units of the average bulk value $b^2N/3$, versus the distance $z$ of the centre of the end-to-end vector from the interface in units of $w_{SSL}$, for homopolymers (long-dashed line) and single copolymer chains (dashed line). The parameters are $\chi = 0.53$, $N = 32$. The points are the corresponding Monte Carlo data. The thick solid line gives the self-consistent-field prediction with capillary-wave correction according to equation (72), with $s^2 = 2.5$ taken from figure 5. From reference [83].

Even though interfaces orient single bonds only very weakly, their effect on whole chains is much stronger. The orientation of whole chains involves two different factors: the orientation of the gyration tensor at constant total gyration radius or end-to-end radius, and stretching or compression of the chain in one direction. The first factor cannot be assessed in a self-consistent-field calculation with Gaussian or nearly Gaussian chains. However, the simulation data shown in figure 7 [83] indicate that the second effect dominates close to an interface: the mean squared components parallel to the interface $xy$ of the end-to-end vectors hardly vary throughout the system, for both homopolymers and copolymers, whereas they strongly depend on the distance from the interface for the $z$-component. Homopolymers are found to be squeezed towards the interface, which leads to an effective parallel orientation. Copolymers show the inverse behaviour: they stretch in the direction perpendicular to the interface. The effect is strongest for copolymers centred between one and two radii of gyration away from the interface, which are pulled towards the interface by their one end, and much weaker for copolymers centred right at the interface, which do not feel strong orienting forces. The latter can be pictured as consisting of two weakly coupled, almost unperturbed homopolymer blocks A and B. Indeed, the end-to-end vectors of single blocks

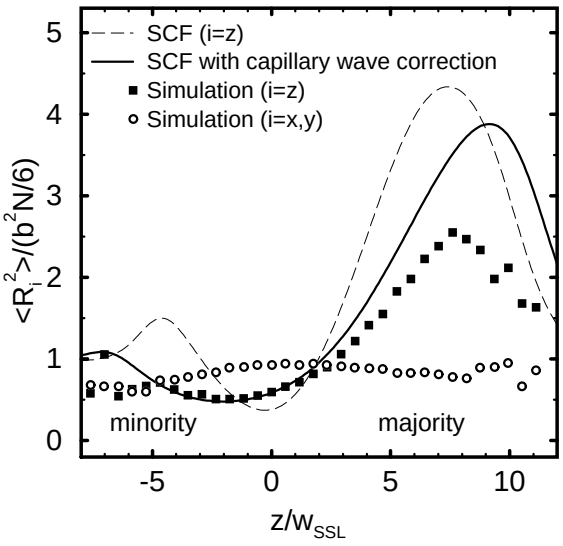


**Figure 8.** The mean square end-to-end vector component $\langle R_i^2 \rangle$ ($i = x, y, z$) of the copolymer blocks in their minority phase (A block in B phase and vice versa) and in their majority phase (A in A, B in B), in units of the average bulk value $b^2N/6$, plotted versus the distance $z$ of the centre of the end-to-end vector from the interface in units of $w_{SSL}$, compared to Monte Carlo data. The parameters are $\chi = 0.53$, $N = 32$. The thick solid line shows the self-consistent-field prediction corrected for capillary waves according to equation (72), with $s^2 = 2.5$ taken from figure 5. From reference [83].

centred at the interface are oriented parallel to the interface, as shown in figure 8.

To conclude, these examples demonstrate that the self-consistent-field theory allows one to study the conformational properties of polymers at interfaces in great detail, and that a wealth of information can be obtained from such calculations. The predictions of the theory were found to be in overall good agreement with Monte Carlo simulations.

### *3.2. Amphiphiles at surfaces*

Our second example deals with a somewhat more exotic application of a self-consistent-field theory, the study of a coarse-grained model for Langmuir monolayers [65, 105]. These are monolayers of amphiphilic molecules adsorbed on a water surface. If the nonpolar chains of the amphiphiles are sufficiently long, one observes experimentally two distinct coexistence regions of two-dimensional fluid phases on increasing the area per molecule (reference [106]): a transition from a highly diluted, 'gas'-like phase (G) into a more condensed, 'liquid expanded' (LE) phase, and a second region at higher surface coverage, where 'liquid condensed' domains are present in a 'liquid expanded' environment. The coexisting high-density phases are true fluid phases, as positional correlations within them decay exponentially within a few nanometres. In contrast, the directions of the bonds connecting nearest-neighbour head groups appear to be correlated over tens of micrometres (reference [107]), which suggests that those phases are probably hexatic. They may be untilted (LS) or tilted (denoted as $L_2$ here), with different directions of tilt. The transition between the liquid expanded and the liquid condensed phase is the monolayer equivalent to the 'main transition' in bilayers, where the bilayer thickness jumps discontinuously as a function of temperature (reference [108]). The latter is probably relevant in biological

systems, because it is found in lipid membranes at temperatures often close to the body temperature (e.g., 41.5 °C in DPPC).

The problem that we wish to address is the following: what is the origin of the first-order transition between these two fluid phases? The onset of bond-orientational order cannot account for the discontinuity, since the transition between a liquid and a hexatic liquid is of Kosterlitz–Thouless type (reference [109]) and thus continuous. There is substantial experimental evidence that the flexibility of the polar tails plays a crucial role. In particular, the liquid expanded phase disappears if the chains are made stiff by replacing the hydrogen atoms with fluorine atoms (reference [110]). The system is thus a good candidate for a self-consistent-field treatment, which takes due account of the conformational degrees of freedom of the chains.

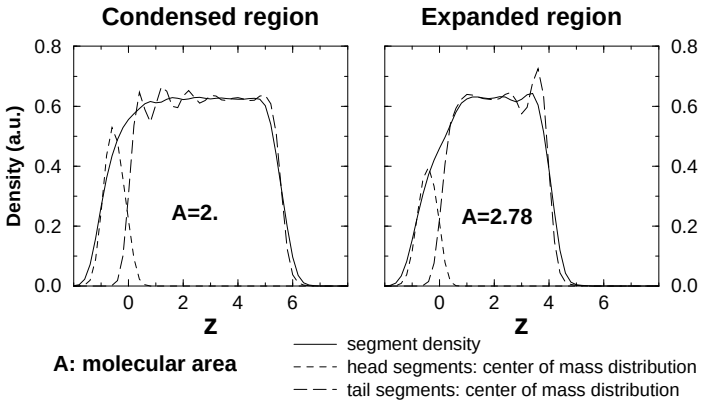


**Figure 9.** Profiles of the density $\rho$ in units of $1/(A_0 l_0)$ versus $z$ in units of $l_0$ for different molecular areas $A/A_0$. Long- and short-dashed lines show the centre-of-mass densities of the tail and head segments, respectively. The solid line shows the coarse-grained density, which accounts for the finite extension of the segments. The parameters are $u = 2$ and $v = 13.7$. From reference [65].

The amphiphiles were modelled as chains containing one head segment, which is confined to a planar surface by a harmonic potential, and seven tail segments of diameter $A_0$ and length $l_0$. The conformational weight is given by an expression of the type (4) with an additional bending stiffness contribution $\exp[u\widehat{U}(\theta)]$, which favours parallel alignment of adjacent segments ($\theta = 0$). The adjustable parameter $u$ determines the stiffness of the chains, and the actual form of $\widehat{U}$ [65] is not of interest here. Chain segments interact via repulsive hard-core and long-range attractive forces. The self-consistent-field treatment of the interactions essentially follows the lines of section 2.3, except that in those short chains, one has to account explicitly for the extended size of the monomers by means of some appropriate coarse graining over the centre-of-mass densities of segments. Furthermore, the interactions have an additional anisotropic component, as may result, for example, from local packing effects. It is included perturbatively by adding an orientation-dependent term

$$\beta\mathcal{V}_{ani} = l_0 A_0 \int \mathrm{d}\boldsymbol{r}\ \mathrm{d}\boldsymbol{u}\ \mathrm{d}\boldsymbol{u}'\ \rho(\boldsymbol{r},\boldsymbol{u})\rho(\boldsymbol{r},\boldsymbol{u}')v\frac{5}{16\pi}(3(\boldsymbol{u}\cdot\boldsymbol{u}')^2-1). \qquad (75)$$

The parameter $v$ is again adjustable and describes the anisotropy per segment of the chains. Within this model, one-dimensional self-consistent-field profiles were calculated in the direction $z$ perpendicular to the surface, and hence the possibility of lateral order (positional order) was not taken into account. Figure 9 shows some typical density profiles. Numerous

other quantities were also evaluated, such as profiles of the nematic tensor, and the in-plane alignment of segments $d_\parallel^2 = \langle u_x \rangle^2 + \langle u_y \rangle^2$, which is only nonzero when the symmetry of the $xy$-plane is broken. The free energy was evaluated according to equation (8), which allows one to calculate phase diagrams by means of a Maxwell construction.

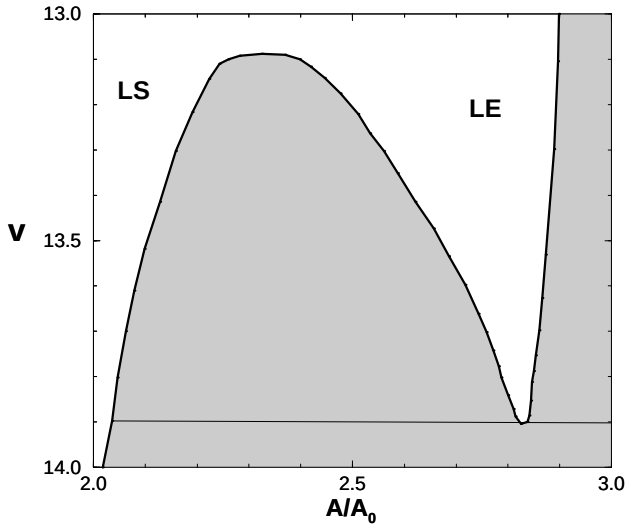


**Figure 10.** The phase diagram for Langmuir monolayers for stiffer chains ($u = 2$) in the plane of anisotropy per segment $v$ versus area per molecule $A$ in units of the chain diameter $A_0$. The shaded area indicates the region of two-phase coexistence. The gas phase is found at much larger values of $A$. Almost the same phase diagram is obtained when varying the stiffness parameter $u$ at fixed anisotropy $v = 13.5$. (The critical point is at $u_c = 1.95$ and the triple point is at $u_t = 2.05$ in arbitrary units.) From reference [65].

One finds that such a model does indeed display coexistence of two untilted fluid phases. The phase behaviour is driven by the stiffness $u$ of the chains (reference [105]), or alternatively by the anisotropic interactions $v$ [65]. On decreasing the interactions or increasing the chain flexibility, the condensed phase merges with the expanded phase at a critical point. On making the chains stiffer or the interactions higher, the expanded phase becomes unstable. Hence the coexistence region ends in a triple point and a critical point, like for experimental Langmuir monolayers (figure 10). In addition, one finds a phase with a uniform tilt in one direction, which is however metastable and buried in the coexistence region (not shown). Since both the effect of segment interactions and the chain stiffness decrease with increasing temperature, the $u$-axis or $v$-axis can be interpreted as a temperature axis.

The nature of the phase transition can thus be analysed. The expanded phase is stabilized by the chain entropy of sufficiently flexible chains. The anisotropic interactions between segments, which have a stronger effect in systems with stiffer chains, are necessary to bring about a distinct condensed phase. The phase transition is driven by the interplay of the entropy of the chains and their tendency towards parallel alignment.

Next, one may ask what happens to the phase diagram (figure 10) if the stiffness $u$ is changed substantially. From the previous results, we can infer that the transition values for $v$ at the critical and triple point are shifted in the opposite direction. In the limit of very stiff chains, the two transitions merge, and one is left with only one first-order

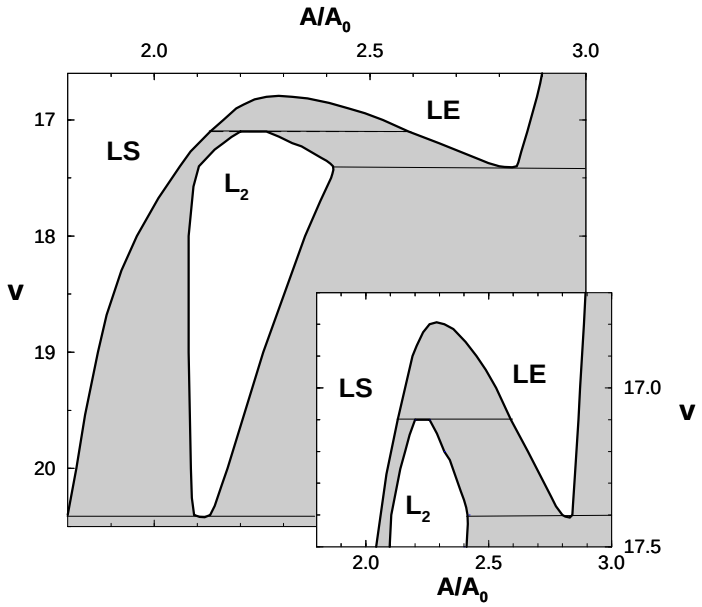


**Figure 11.** The phase diagram for Langmuir monolayers for flexible chains ($u = 1.5$) in the plane of anisotropy per segment $v$ versus area per molecule $A$ in units of chain diameter $A_0$. The $L_2$ region corresponds to a phase with broken symmetry in the $xy$-plane, where the chains are collectively tilted in one direction. From reference [65].

transition, from the gas phase directly into the untilted condensed phase. This agrees with the experimental results of reference [110]. If the chains are made more flexible, on the other hand, the already mentioned tilted phase emerges as an additional stable phase: the gain of conformational entropy at the corresponding surface densities compensates in part for the loss of surface energy per chain, and surface coverages are stabilized which support collective tilt. This is illustrated in figure 11. The liquid expanded phase can then coexist with either an untilted condensed phase or a tilted condensed phase. At even higher chain flexibility, the coexisting condensed phase is entirely tilted, and turns into an untilted phase via a continuous transition upon further compression of the monolayer (not shown). Hence tilted phases are stabilized by chain flexibility. Note however that other tilting mechanisms are possible (e.g., resulting from a mismatch between the head size and chain diameter), which are presumably predominant in real monolayers.

In summary, the self-consistent-field analysis of this model lays open a rich and complex phenomenology. The different phases at low surface coverage are largely recovered. This demonstrates again the power of the method even for systems with relatively short chains, even though, unlike in polymers, the predictions cannot be expected to be quantitative here.

## 4. Forward look

We have reviewed some recent advances in the self-consistent-field approach, with the aim of giving a flavour of the potential and the limitations of this method in the study of complex fluids. Many paths of further development are possible. For example, the combination of self-consistent-field theories with other more microscopic mean-field approaches, like the P-RISM theory [75], might open up promising routes for tackling new topical problems

like polymer crystallization. In general, the investigation of interrelations between different mean-field approaches contributes to a deepened understanding of the individual methods (references [111, 112]). Another challenging problem for the future is the formulation of a general self-consistent-field theory for semidilute self-avoiding chains, which would bridge between the self-avoiding-chain statistics on small length scales and the random-walk-chain statistics on larger length scales (reference [57] is a first attempt in this direction). Such a method would allow one, for example, to study interfaces between hydrophobic and hydrophilic polymer components in aqueous environments, which are of great interest in biology.

## Acknowledgments

I wish to thank M Schick, A Werner, M Müller, P Janert and K Binder for fruitful and enjoyable collaborations, and M W Matsen and P Nielaba for stimulating discussions. Partial financial support by the Deutsche Forschungsgemeinschaft (grants Schm 985/1-1 and Bi 314/3-4), by the Materialwissenschaftliches Forschungszentrum Mainz (MWFZ) and by the Graduiertenkolleg on Supramolecular Systems in Mainz is acknowledged.

## References

[1] Wu S 1982 *Polymer Interfaces and Adhesion* (New York: Dekker)
[2] Garbassi F, Morra M and Occhiello E 1994 *Polymer Surfaces from Physics to Technology* (Chichester: Wiley)
[3] Mayes A M and Kumar S K 1997 *MRS Bull.* **22** 43
[4] Geary J M, Goodby J W, Kmetz A R and Patel J S 1987 *J. Appl. Phys.* **62** 4100
[5] Willson C G 1994 *Introduction to Micro-lithography* ed L F Thompson, C G Willson and M J Bowden (Washington, DC: American Chemical Society) p 139
[6] Hildebrand J H and Scott R L 1964 *The Solubility of Non-electrolytes* (New York: Dover)
[7] Wu S 1987 *Polym. Eng. Sci.* **27** 335
[8] Wool R P 1995 *Polymer Interfaces* (Munich: Hanser)
[9] Schnell R, Stamm M and Creton C 1998 *Macromolecules* **31** 2284
[10] Bates F S and Fredrickson G H 1990 *Annu. Rev. Phys. Chem.* **41** 512
Bates F S, Schulz M F, Khandpur A K, Förster S, Rosedale J H, Almdal K and Mortensen K 1994 *Faraday Discuss.* **98** 7
[11] Bates F S 1991 *Science* **251** 898
[12] Templin M, Franck A, Chesne U, Leist H, Zhang Y, Ulrich R, Schädler V and Wiesner U 1997 *Science* **278** 1795
[13] Anastasiadis S H, Gancarz I and Koberstein J T 1989 *Macromolecules* **22** 1449
[14] Beck Tan N C, Tai S-K and Briber R M 1997 *Polymer* **37** 3509
[15] Milner S T and Xi H 1996 *J. Rheol.* **40** 663
Milner S T 1997 *MRS Bull.* **22** 38
[16] Kinning D J, Winey K I and Thomas E L 1988 *Macromolecules* **21** 3502
Kinning D J 1989 *J. Chem. Phys.* **90** 5806
Winey K I, Thomas E L and Fetters L J 1991 *J. Chem. Phys.* **90** 9367
Bates F S, Maurer W W, Lipic P M, Hillmyer P M A, Almdal K, Mortensen K, Fredrickson G H and Lodge T P 1997 *Phys. Rev. Lett.* **79** 849
[17] Leibler L and Pincus P A 1984 *Macromolecules* **17** 2922
Semenov A N 1993 *Macromolecules* **26** 2273
Matsen M W and Bates F S 1996 *Macromolecules* **29** 1091
[18] Luzzati V, Tradieu A, Gulik-Krzywicki T, Rivas E and Reiss-Husson F 1968 *Nature* **220** 485
[19] Gompper G and Schick M 1994 Self-assembling amphiphilic systems *Phase Transitions and Critical Phenomena* vol 16, ed C Domb and J L Lebowitz (London: Academic)
[20] Flory P 1971 *Principles of Polymer Chemistry* (Ithaca, NY: Cornell University Press)
[21] de Gennes P G 1979 *Scaling Concepts in Polymer Physics* (Ithaca, NY: Cornell University Press)

[22] Freed K F 1987 *Renormalization Group Theory of Macromolecules* (New York: Wiley–Interscience)
[23] Ginzburg V L 1960 *Sov. Phys.–Solid State* **1** 1824
de Gennes P-G 1977 *J. Physique Lett.* **38** L441
Joanny J F 1978 *J. Phys. A: Math. Gen.* **11** L117
Binder K 1984 *Phys. Rev.* A **29** 341
[24] For a recent review on Ginzburg–Landau approaches to polymer systems, see
Holyst R and Vilgis T A 1996 *Macromol. Theory Simul.* **5** 573
[25] Flory P J 1941 *J. Chem. Phys.* **9** 660
Huggins H L 1941 *J. Chem. Phys.* **9** 440
[26] Dudowicz J and Freed K F 1990 *Macromolecules* **23** 1519
Lifshitz M and Freed K F 1993 *J. Chem. Phys.* **98** 8994
Foreman K W and Freed K F 1995 *J. Chem. Phys.* **102** 4663
[27] Aguilera-Granja F and Kikuchi R 1990 *Physica* A **176** 514
Aguilera-Granja F and Kikuchi R 1991 *Physica* **182** 331
Aguilera-Granja F and Kikuchi R 1992 *Physica* **189** 81
Aguilera-Granja F and Kikuchi R 1992 *Physica* **189** 108
[28] McMullen W E and Freed K F 1990 *J. Chem. Phys.* **92** 1413
Tang H and Freed K F 1991 *J. Chem. Phys.* **94** 1572
McMullen W E and Trache M 1994 *J. Chem. Phys.* **102** 1440
[29] Woodward C E 1991 *J. Chem. Phys.* **94** 3193
Woodward C E 1992 *J. Chem. Phys.* **97** 4527
Woodward C E and Yethiray A 1993 *J. Chem. Phys.* **100** 3181
[30] Chandler D, McCoy J D and Singer S J 1986 *J. Chem. Phys.* **85** 5971
Sen S, Cohen J M, McCoy J D and Curro J G 1994 *J. Chem. Phys.* **101** 9010
Sen S, McCoy J D, Nath M K, Donley J P and Curro J G 1994 *J. Chem. Phys.* **102** 3431
[31] Kierlik E and Rosinberg M L 1994 *J. Chem. Phys.* **100** 1716
[32] Helfand E and Tagami Y 1971 *J. Polym. Sci.* B **9** 741
Helfand E 1971 *J. Chem. Phys.* **56** 3592
Helfand E 1972 *J. Chem. Phys.* **57** 1812
[33] Helfand E and Sapse A M 1975 *J. Chem. Phys.* **62** 1327
Helfand E 1975 *J. Chem. Phys.* **62** 999
[34] Hong K M and Noolandi J 1981 *Macromolecules* **14** 727
Hong K M and Noolandi J 1981 *Macromolecules* **14** 737
[35] Shull K R and Kramer E J 1990 *Macromolecules* **23** 4769
Shull K R 1991 *Macromolecules* **25** 2122
Shull K R 1993 *Macromolecules* **26** 2346
[36] Scheutjens J M H M and Fleer G J 1979 *J. Chem. Phys.* **83** 1619
[37] Pesci A I and Freed K F 1989 *J. Chem. Phys.* **90** 2003
Pesci A I and Freed K F 1989 *J. Chem. Phys.* **90** 2017
Dudowicz J and Freed K F 1991 *Macromolecules* **24** 5076
Dudowicz J and Freed K F 1991 *Macromolecules* **24** 5096
Dudowicz J and Freed K F 1991 *Macromolecules* **24** 5112
Foreman K W, Freed K F and Ngola I M 1997 *J. Chem. Phys.* **107** 4688
For a recent review, see
Foreman K W and Freed K F 1998 *Adv. Chem. Phys.* **103** 335
[38] For a recent review on P-RISM theory, see
Schweizer K S and Curro J G 1997 *Advances in Chemical Physics* vol XCVIII, ed I Prigogine and S A Rice (New York: Wiley) p 1
[39] Edwards S F 1965 *Proc. Phys. Soc.* **85** 613
[40] Cosgrove T, Vincent B, Scheutjens J M H M, Fleer G J and Cohen-Stuart M A 1993 *Polymers at Interfaces* (London: Chapman and Hall)
[41] Binder K (ed) 1995 *Monte Carlo and Molecular Dynamics Simulations in Polymer Science* (New York: Oxford University Press)
[42] Binder K 1994 *Adv. Polym. Sci.* **112** 181
Binder K 1998 *Adv. Polym. Sci.* at press
Binder K 1995 *Acta Polym.* **46** 204
[43] Carmesin I and Kremer K 1988 *Macromolecules* **21** 2819
Deutsch H-P and Binder K 1991 *J. Chem. Phys.* **94** 2294

[44] For a recent review on Monte Carlo simulations of polymer interfaces, see
Müller M and Schmid F 1998 *Annual Reviews of Computational Physics VI* (Singapore: World Scientific) at press
[45] Matsen M W and Schick M 1994 *Macromolecules* **27** 6761
[46] Müller M and Werner A 1997 *J. Chem. Phys.* **107** 10 764
[47] Helfand E 1975 *J. Chem. Phys.* **62** 999
[48] Kratky O and Porod G 1949 *Rec. Trav. Chim.* **68** 1106
Saito N, Takahashi K and Yuniki Y 1967 *J. Phys. Soc. Japan* **22** 219
[49] Morse D C and Fredrickson G H 1994 *Phys. Rev. Lett.* **73** 3235
[50] Carignano M A and Szleifer I 1993 *J. Chem. Phys.* **98** 5006
Carignano M A 1995 *Macromolecules* **28** 3197
[51] For recent reviews on the Szleifer method, see
Szleifer I and Carignano M A 1996 *Advances in Chemical Physics* vol XCIV, ed I Prigogine and S A Rice (New York: Wiley) p 165
Szleifer I 1997 *Curr. Opin. Colloid Interface Sci.* **1** 416
[52] Matsen M W 1995 *Phys. Rev. Lett.* **74** 4225
[53] Shi A-C, Noolandi J and Desai R C 1996 *Macromolecules* **29** 6487
[54] Laradji M, Shi A-C, Noolandi J and Desai R C 1997 *Phys. Rev. Lett.* **78** 2577
Laradji M, Shi A-C, Noolandi J and Desai R C 1997 *Macromolecules* **30** 3242
[55] Matsen M W 1998 *Phys. Rev. Lett.* **80** 4470
[56] Berg B A and Neuhaus T 1989 *Phys. Rev. Lett.* **68** 9
Berg B A and Neuhaus T 1991 *Phys. Lett.* **267B** 249
[57] Weinhold J D, Kumar S K and Szleifer I 1996 *Europhys. Lett.* **35** 695
[58] Müller M 1998 at press
[59] Matsen M W and Schick M 1994 *Phys. Rev. Lett.* **72** 2660
[60] Matsen M W 1997 *J. Chem. Phys.* **106** 7781
[61] For recent reviews on applications of the self-consistent-field theory in the study of ordered block-copolymer phases, see
Matsen M W and Bates F S 1996 *Macromolecules* **29** 1091
Matsen M W and Schick M 1996 *Curr. Opin. Colloid Interface Sci.* **1** 329
Matsen M W 1998 *Curr. Opin. Colloid Interface Sci.* **3** 40
[62] Schmid F and Müller M 1995 *Macromolecules* **28** 8641
[63] Press W H, Flannery B P, Teukolsky S A and Vetterling W T 1988 *Numerical Recipes* (Cambridge: Cambridge University Press)
[64] Ng K-C 1974 *J. Chem. Phys.* **61** 2680
[65] Schmid F 1997 *Phys. Rev.* E **55** 5774
[66] Dennis J E and Schnabel R B 1983 *Numerical Methods for Unconstrained Optimization and Nonlinear Equations* (Englewood Cliffs, NJ: Prentice-Hall)
[67] Janert P 1997 *PhD Thesis* University of Washington, Seattle, WA
[68] Theodorou D N 1989 *Macromolecules* **22** 4578
Theodorou D N 1989 *Macromolecules* **22** 4589
[69] Hariharan A, Kumar S K and Russell T P 1993 *J. Chem. Phys.* **98** 4163
Hariharan A, Kumar S K and Russell T P 1993 *J. Chem. Phys.* **99** 4041
Hariharan A and Harris J G 1994 *J. Chem. Phys.* **101** 3353
[70] Sanchez I C and Lacombe R H 1978 *Macromolecules* **11** 1145
[71] Deutsch H-P and Dickman R 1990 *J. Chem. Phys.* **93** 8983
[72] Schmid F 1996 *J. Chem. Phys.* **104** 9191
[73] Dickman R and Hall C K 1986 *J. Chem. Phys.* **85** 4108
[74] Dee G T and Walsh D J 1988 *Macromolecules* **21** 811
Nies E and Stroeks A 1990 *Macromolecules* **23** 4088
Lipson J E G and Andrew S S 1992 *J. Chem. Phys.* **96** 1426
[75] Nath S K, McCoy J D, Donley J P and Curro J G 1995 *J. Chem. Phys.* **103** 1635
[76] Hansen J-P and McDonald I R 1990 *Theory of Simple Liquids* (London: Academic)
[77] In some cases, it may be more convenient to work with the indirect correlation function $y(\boldsymbol{r}) = \exp[\beta W_0(\boldsymbol{r})]\gamma(\boldsymbol{r})$, which has the advantage of being continuous even in hard-core systems, and to replace $U_{\alpha\beta}(\boldsymbol{r})$ in equation (44) by $\tilde{U}_{\alpha\beta}(\boldsymbol{r}) = \exp[-\beta W_0(\boldsymbol{r})] - \exp[-\beta W_{\alpha\beta}(\boldsymbol{r})]$.
[78] Paul W, Binder K, Heermann D W and Kremer K 1991 *J. Chem. Phys.* **95** 7726
[79] Müller M and Paul W 1993 *J. Chem. Phys.* **100** 719

[80] Müller M and Binder K 1995 *Macromolecules* **28** 1825
Müller M 1995 *Macromolecules* **28** 6556
[81] Rouault Y, Dünweg B, Baschnagel J and Binder K 1996 *Polymer* **37** 297
[82] Müller M, Binder K and Oed W 1995 *J. Chem. Soc. Faraday Trans.* **91** 3269
[83] Werner A, Schmid F, Binder K and Müller M 1996 *Macromolecules* **29** 9241
[84] Maurer W W, Bates F S, Lodge T P, Almdal K, Mortensen K and Fredrickson G H 1998 *J. Chem. Phys.* **108** 2989
[85] Buff F P, Lovett R A and Stillinger F H 1965 *Phys. Rev. Lett.* **15** 621
Weeks J D 1977 *J. Chem. Phys.* **67** 3106
Bedeaux D and Weeks J D 1985 *J. Chem. Phys.* **82** 972
[86] Shull K R, Mayes A M and Russell T P 1993 *Macromolecules* **26** 3929
[87] Semenov A N 1993 *Macromolecules* **26** 6617
Semenov A N 1994 *Macromolecules* **27** 2732
[88] Kerle T, Klein J and Binder K 1996 *Phys. Rev. Lett.* **77** 1318
Kerle T, Klein J and Binder K 1998 *Eur. Phys. J.* at press
[89] Sferrazza M, Xiao C, Jones R A L, Bucknall D G, Webster J and Penfold J 1997 *Phys. Rev. Lett.* **78** 3693
[90] Jasnow D 1984 *Rep. Prog. Phys.* **47** 1059
[91] Werner A, Schmid F, Müller M and Binder K 1997 *J. Chem. Phys.* **107** 8175
[92] Werner A 1998 *PhD Thesis* University of Mainz
[93] Werner A, Schmid F, Müller M and Binder K 1998 *Preprint*
[94] Janert P K and Schick M 1997 *Macromolecules* **30** 137
Janert P K and Schick M 1997 *Macromolecules* **30** 3916
[95] Noolandi J and Hong K M 1981 *Macromolecules* **15** 482
Noolandi J and Hong K M 1984 *Macromolecules* **17** 1531
Noolandi J, Shi A-C and Linse P 1996 *Macromolecules* **29** 5907
[96] Fischel L B and Theodorou D N 1995 *J. Chem. Soc. Faraday Trans.* **91** 2381
[97] Balasz A C, Gersappe D, Israels R and Fasolka M 1995 *Macromol. Theory Simul.* **4** 585
Israels R, Jasnow D, Balasz A C, Guo L, Krausch G, Sokolov J and Rafailovich M 1995 *J. Chem. Phys.* **102** 8149
[98] Genzer J, Faldi A and Composto R J 1994 *Phys. Rev.* E **50** 2373
[99] Müller M and Binder K 1998 *Macromolecules* at press
[100] Fleer G J and Leermakers F A M 1997 *Curr. Opin. Colloid Interface Sci.* **2** 308
[101] Huang K and Balasz A C 1991 *Phys. Rev. Lett.* **66** 620
Huang K and Balasz A C 1993 *Macromolecules* **26** 4736
Zhulina E, Singh C and Balasz A C 1996 *Macromolecules* **29** 6338
Zhulina E, Singh C and Balasz A C 1996 *Macromolecules* **29** 8254
[102] Sanchez I C (ed) 1992 *Physics of Polymer Surfaces and Interfaces* (Boston, MA: Butterworth–Heinemann)
[103] Here the broadening parameter $s^2$ was used as an adjustable parameter ($s^2 = 2.5$). The actual size of the simulation box was $L \times L \times D$ with $L = 512$ and $D = 64$. However, the capillary-wave spectrum here is limited neither by $L$ nor by $D$, but by the time needed for capillary waves to build up. In systems with purely diffusive dynamics, the relaxation time for long-wavelength capillary waves slows down dramatically with $1/q$ ($t \propto q^{-4}$; reference [104]). This effectively cuts them off at some value $q_{\min}$, which depends only weakly on the total simulation period after an initial relaxation time, and which is found to be $q_{\min}^{-1} \approx 60$ in our case. For the detailed study of capillary-wave effects in reference [91], smaller systems had to be studied, and nonlocal Monte Carlo moves were used.
[104] Müller M 1998 private communication
[105] Schmid F and Schick M 1995 *J. Chem. Phys.* **102** 2080
[106] Knobler C M 1990 *Science* **249** 870
Möhwald H 1990 *Annu. Rev. Phys. Chem.* **41** 441
McConnell H M 1991 *Annu. Rev. Phys. Chem.* **42** 171
Knobler C M and Desai R C 1992 *Annu. Rev. Phys. Chem.* **43** 207
Kaganer V M, Möhwald H and Dutta P 1998 *Rev. Mod. Phys.* at press
[107] Helm C A, Möhwald H, Kjaer K and Als-Nielsen J 1987 *Biophys. J.* **52** 381
Kjaer K, Als-Nielsen J, Helm C A, Laxhuber L A and Möhwald H 1987 *Phys. Rev. Lett.* **58** 2224
[108] For a review on bilayers, see, e.g.,
Bloom M, Evans E and Mouritsen O G 1991 *Q. Rev. Biophys.* **24** 293
[109] Halperin B I and Nelson D R 1978 *Phys. Rev. Lett.* **41** 121
[110] Barton S W, Goudot A, Bouloussa O, Rondelez F, Lin B, Novak F, Acero A and Rice S A 1992 *J. Chem.*

*Phys.* **96** 1343
Li M, Acero A A, Huang Z and Rice S A 1994 *Nature* **367** 151
[111] Freed K F 1995 *J. Chem. Phys.* **103** 3230
Freed K F 1996 *J. Chem. Phys.* **105** 10 572
[112] Donley J P, Rajasekaran J J, McCoy J D and Curro J G 1995 *J. Chem. Phys.* **103** 5061